Geodetic techniques

- Triangulation
- Leveling transect
- Trilateration
- VLBI (Very Long Baseline Interferometry)
- SLR (Satellite Laser Ranging)
- GPS (Global Positioning System)
- InSAR (Interferometric Synthetic Aperture Radar)

could add absolute gravity as a potential means to learn of things too.

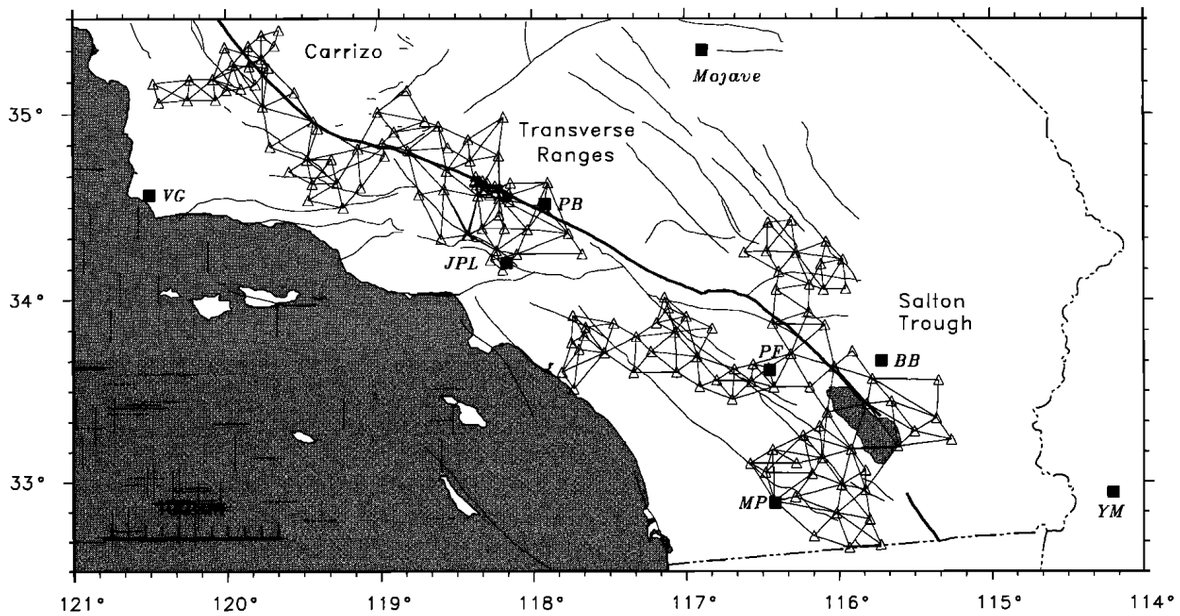

Fig. 1. Trilateration networks in southern California. VLBI stations are shown by solid squares. Stations identified by initials are VG, Vandenburg; JPL, Jet Propulsion Lab; PB, Pearblossom; PF, Pinyon Flat; MP, Monument Peak; BB, Black Butte; and YM, Yuma. Principal faults are shown by sinuous lines. The San Andreas fault and the Imperial fault are shown by heavy sinuous lines.

Lisowski et al., JGR, 1991

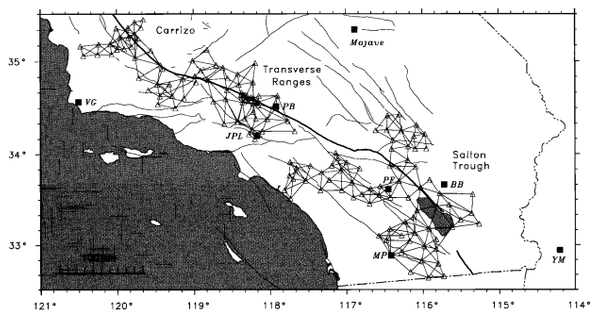

Fig. 1. Trilateration networks in southern California. VLBI stations are shown by solid squares. Stations identified by initials are VG, Vandenburg; JPL, Jet Propulsion Lab; PB, Pearblossom; PF, Pinyon Flat; MP, Monument Peak; BB, Black Butte; and YM, Yuma. Principal faults are shown by sinuous lines. The San Andreas fault and the Imperial fault are shown by heavy sinuous lines.

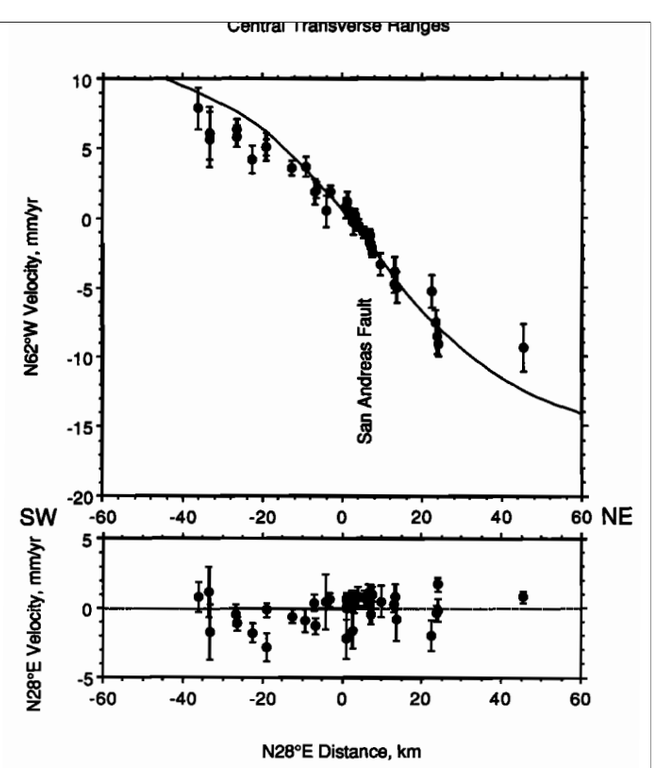

Fig. 10. Horizontal velocity components perpendicular (top) and parallel (bottom) to a N28°E profile across the central Transverse Ranges as a function of distance along the profile. The error bars represent one standard deviation on either side of the plotted point. The continuous line represents the veolicty profile predicted by the one-dislocation half–space model [*Savage, 1990*].

Lisowski et al., JGR, 1991

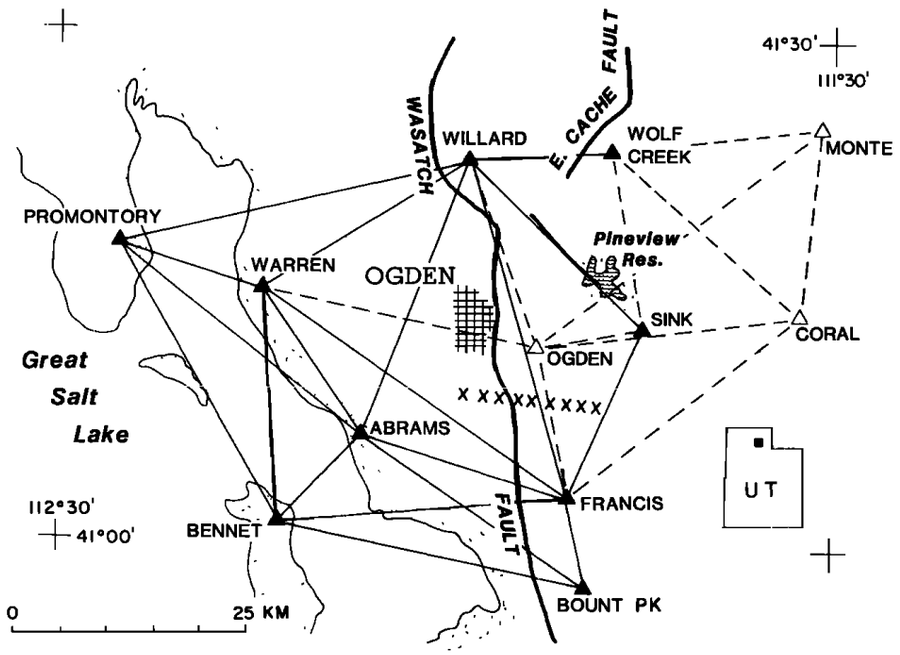

Fig. 5. Ogden strain network. The solid lines and solid triangles represent the original network established in 1972, whereas the dashed lines and open triangles represent the 1981 additions to the network. The line of crosses across the Wasatch fault near the center of the network represents the short level line in Weber canyon.

Savage et al., JGR, 1985

Strain networks were established in many areas, this one across the Wasatch Fault (the fault G K Gilbert warned about in the 1880s).

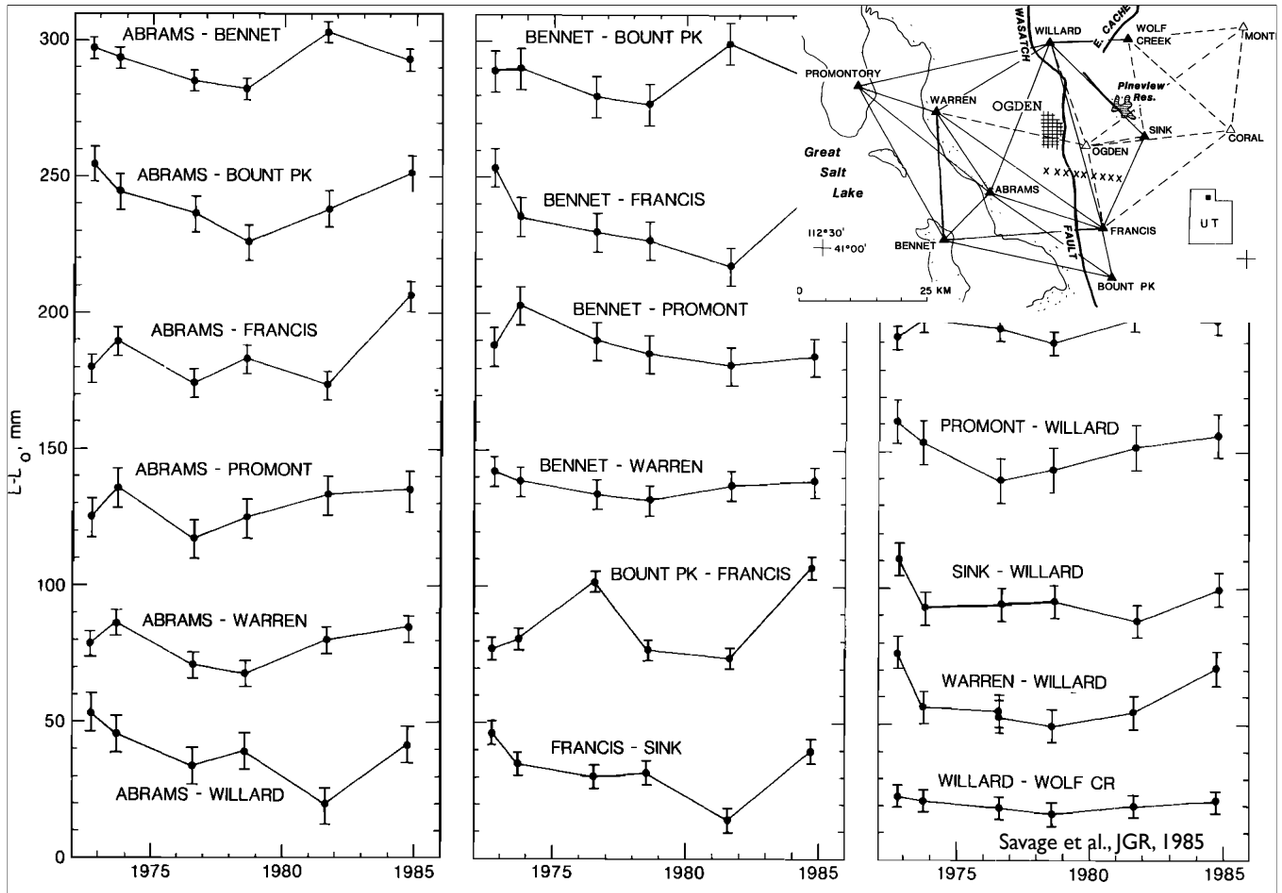

Fig. 6. Line length L (less a constant nominal length L_0) as a function of time for each of the lines in the original (solid lines in Figure 5) Ogden network. The error bars represent 1 standard deviation on either side of the plotted point.

Across the Wasatch Fault, not so much showing up—strain rate estimate not different from 0 in this case.

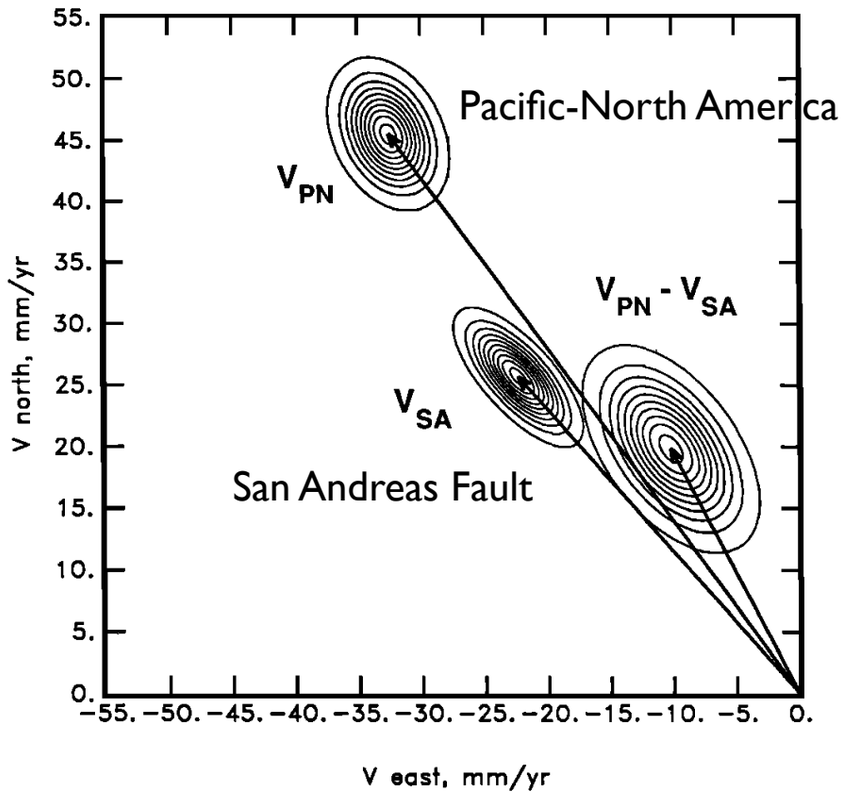

Minster and Jordan, *JGR*, 1987

Reproducing the Minster and Jordan 1984 result that suggested there was a big discrepancy between the San Andreas and global plate circuit estimates. At the time this was found, a VLBI station in the northern Sierra was thought to move with NAM--later determined this was the antenna slowly falling over (plus it is near some strike-slip faults cutting across the northern Sierra). Where this discrepancy was was a big issue in the late 1980s

Mojave Desert geodesy

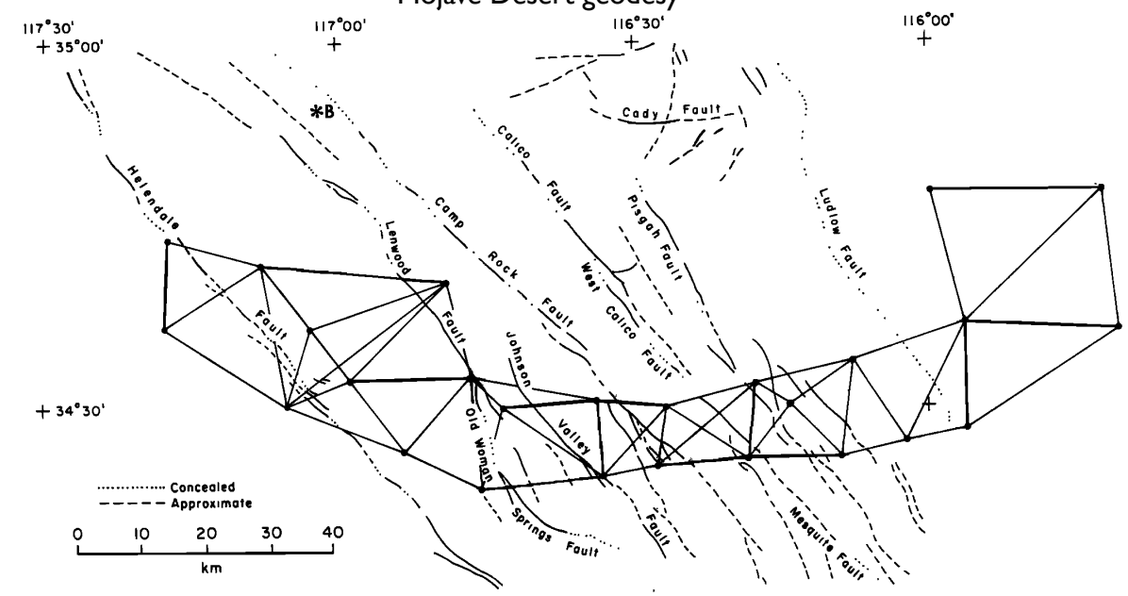

TABLE 1. Rate and Orientation of Maximum Right-Lateral Shear Strain, Mojave Network, 1934–1982

	Western Region	Eastern Region
Number of angles	64	59
$\dot{\gamma}_1$, μstrain/yr	0.16 ± 0.03	0.02 ± 0.04
$\dot{\gamma}_2$, μstrain/yr	-0.02 ± 0.03	0.04 ± 0.03
$\dot{\gamma}$, μstrain/yr	0.16 ± 0.03	0.05 ± 0.03
ψ	N41°W ± 5°	unresolvable

Rates at left amount to 6.7 ± 1.3 mm/yr

Sauber et al., *JGR*, 1986

First recognition that the active branch of the plate boundary missing in the VLBI measurements was in the Basin and Range came from this study of another geodetic network that attracted a lot less attention.

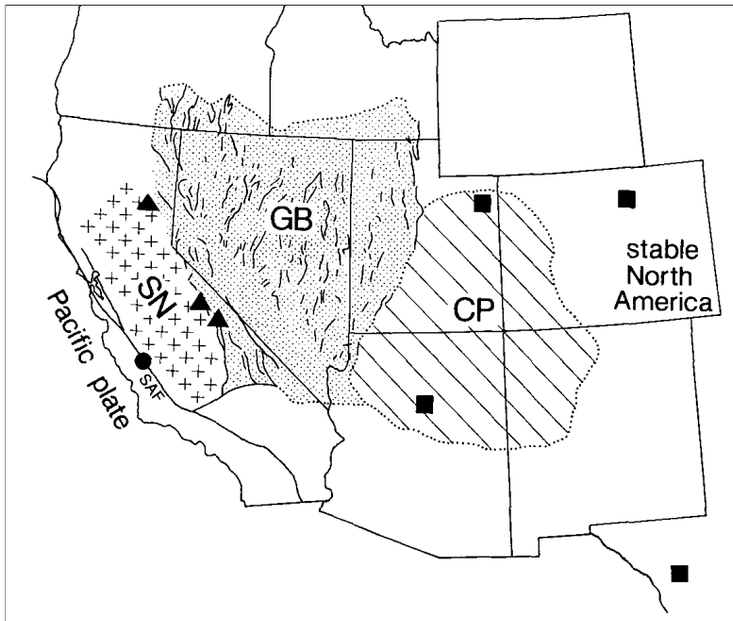

Figure 1. Simplified tectonic map of western United States. We assume that Sierra Nevada and Great Valley of eastern and central California compose Sierra Nevadan (SN) microplate. We furthermore assume that Colorado Plateau (CP) and stable North America compose North American plate. Physiography defines limits of Great Basin (GB), a zone of distributed deformation between the two plates. Quaternary faults of Great Basin are from Zoback (1989, Fig. 3). Radio telescope sites on North American plate (solid squares) are Fort Davis (Texas), Platteville (Colorado), Flagstaff (Arizona), and Vernal (Utah). Radio telescope sites along eastern margin of Sierra Nevadan microplate (solid triangles) that were used to determine its motion are, from north to south, Quincy, Mammoth Lakes, and Owens Valley, California. Solid circle is located at lat 36°N along San Andreas fault (SAF).

Argus and Gordon, Geology, 1991

Other VLBI-based attempts added in Owens Valley Radio Observatory as a point to represent the Sierra…

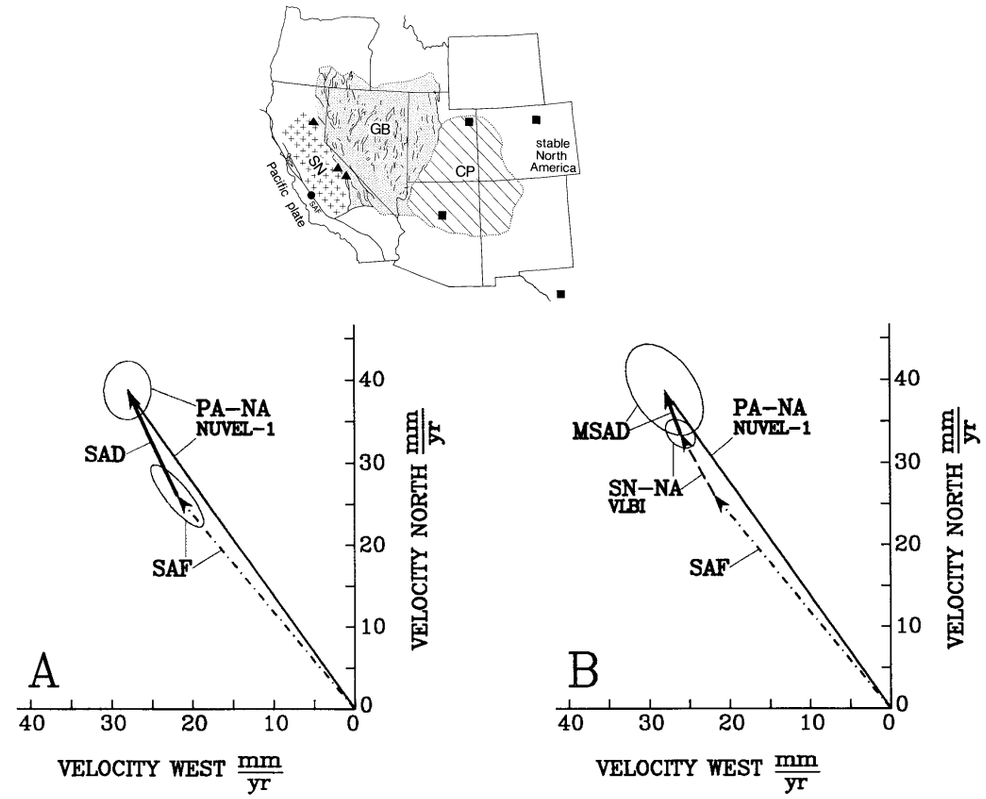

Figure 2. Linear velocity vectors along San Andreas fault at lat 36°N. A: Slip along San Andreas fault (SAF; alternating dash-dot vector) takes up only part of Pacific–North America motion predicted by global-plate-motion model NUVEL-1 (thin solid vector). Vector difference between the two, termed San Andreas discrepancy (SAD; thick solid vector), equals 14 ±2 mm/yr toward N26° ±6°W. Circle and ellipse indicate 95% confidence limits for San Andreas fault slip and for Pacific–North America (PA-NA) motion. B: Vector sum of strike slip along San Andreas fault and Sierra Nevada–North America motion (SN-NA; dashed vector; VLBI = very long baseline interferometry) differs little from Pacific– North America motion. Modified San Andreas discrepancy (MSAD), which equals difference between these two quantities, is 6 ±2 mm/yr toward N20° ±17°W. Ellipses indicate 95% confidence limits for Sierra Nevada–North America motion and for modified San Andreas discrepancy.

Argus and Gordon, Geology, 1991

..this in essence closed the gap. Most if not all of the discrepancy was on the east side of the Sierra.

GPS geodesy: some signals

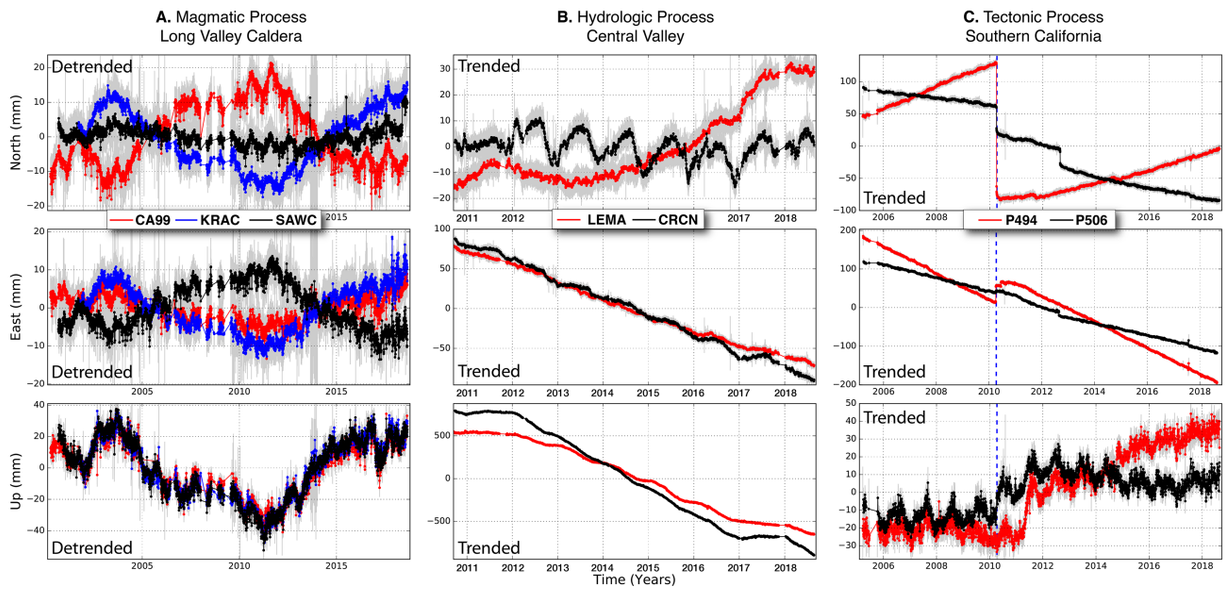

Klein et al., JGR, 2019

Now of course VLBI is supplanted with GPS geodesy; these are a few of the kinds of signals that can be of interest. Note the scale on the vertical for panel b.

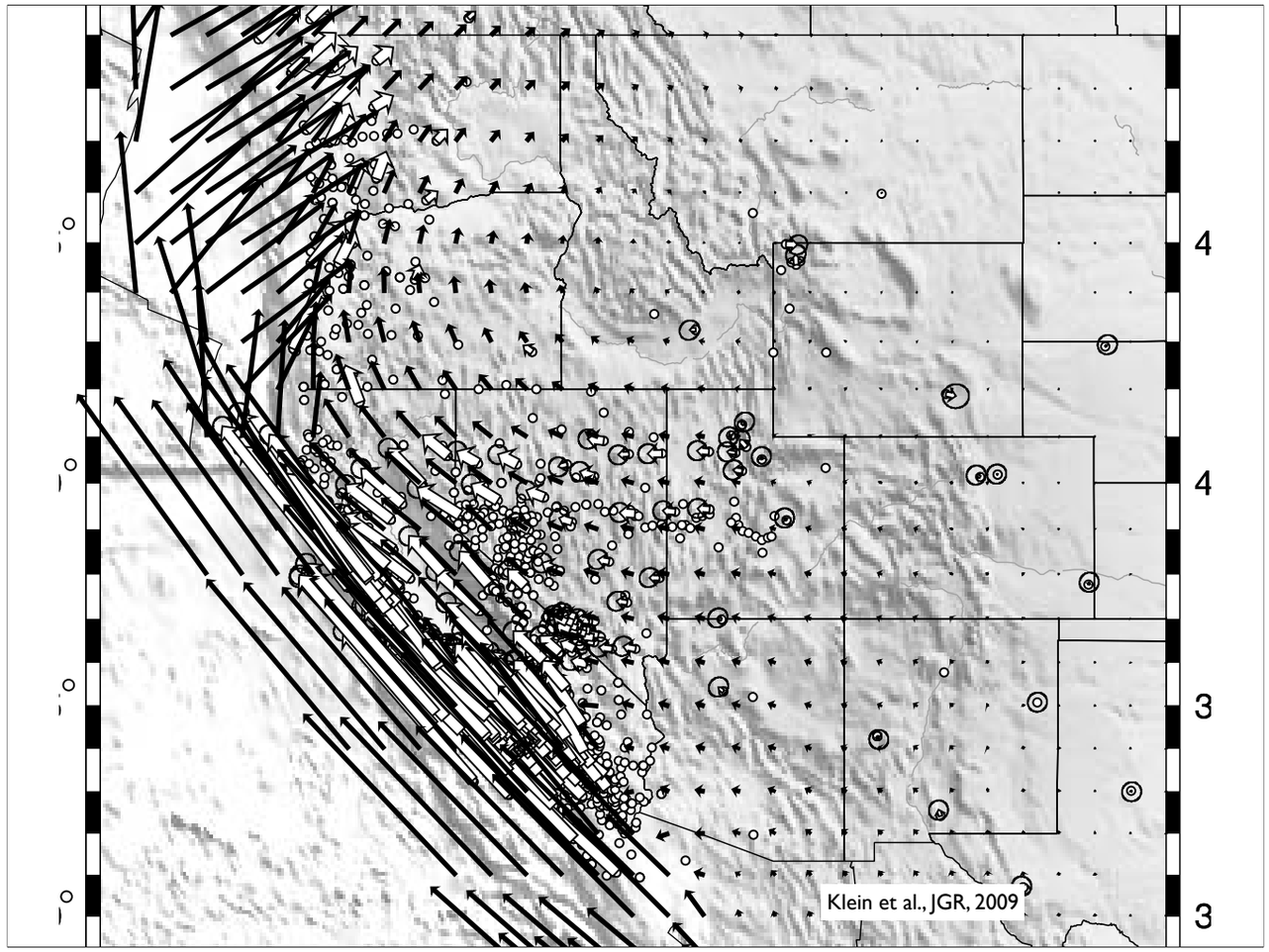

Now of course VLBI is supplanted with GPS geodesy--open arrows/dots are actual points

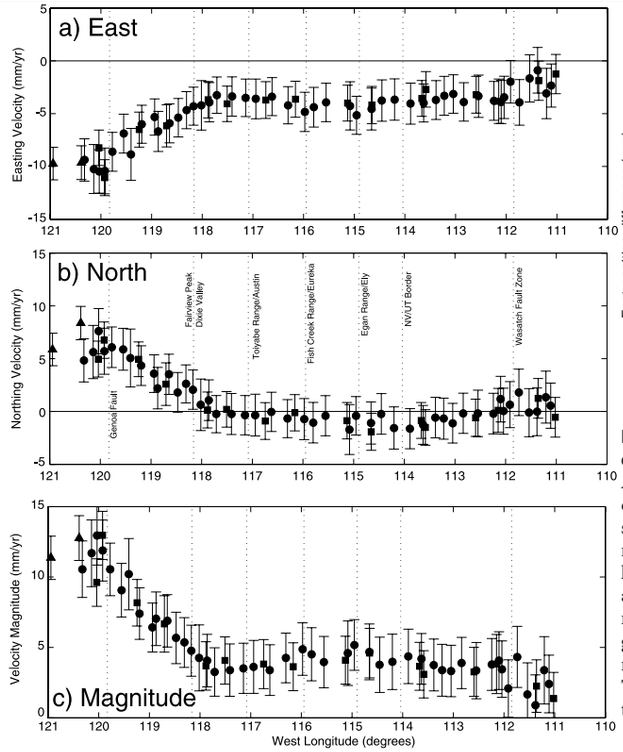

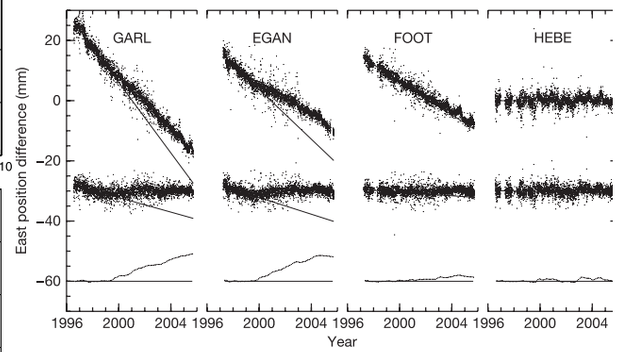

Figure 2 | Illustration of the post-analysis procedure, using time series o east position for four BARGEN sites. Top, 'raw' time series, in a North America-fixed geodetic reference frame (see Methods). Error bars are omitted for clarity, but are generally ~1 mm. The straight line is the best-fi straight line using position estimates from the first 2.5 years. Middle, residuals of the raw time series from a best-fit model consisting of a straigh line and seasonal (annual and semi-annual sinusoids) terms. A statistical approach that allowed these terms to change with time in a constrained manner was used (see Methods). Bottom, residuals smoothed with a gaussian filter with a full-width at half-maximum (FWHM) of ~8 months. A model based on a linear fit to the first 2.5 years of data has been removed. The evolution of these final time series thus indicates deviation from temporally linear motion.

Davis et al., Nature, 2006

Figure 2. (a) East component, (b) north component, and (c) magnitude of velocity with respect to North America. The error bars indicate 2σ uncertainty. Vertical dotted lines show longitude of the indicated fault or geographic feature, squares are off-axis sites, circles are on-axis sites, and triangles are the sites QUIN (near 121°W) and CMBB (near 120.5°W) on the SNGV. (d) Relative plate motion normal component $V_{\perp}$, i.e., component of GPS velocity that lies along the great circle between the Pacific–North America pole of rotation and the GPS site, positive to the northeast, (e) relative plate motion parallel component $V_{//}$, i.e., the horizontal component tangent to the small circle around the pole, positive northwest, and (f) geographic azimuth of velocity, measured as degrees clockwise from north. Horizontal axis is distance from the center of the network projected along the great circle connecting the Pacific–North America pole and the center of the network. Other symbols are as in the previous figure.

Hammond & Thatcher, JGR, 2004

Pros and cons of lots of data in space (left) and time (BARGEN, right).

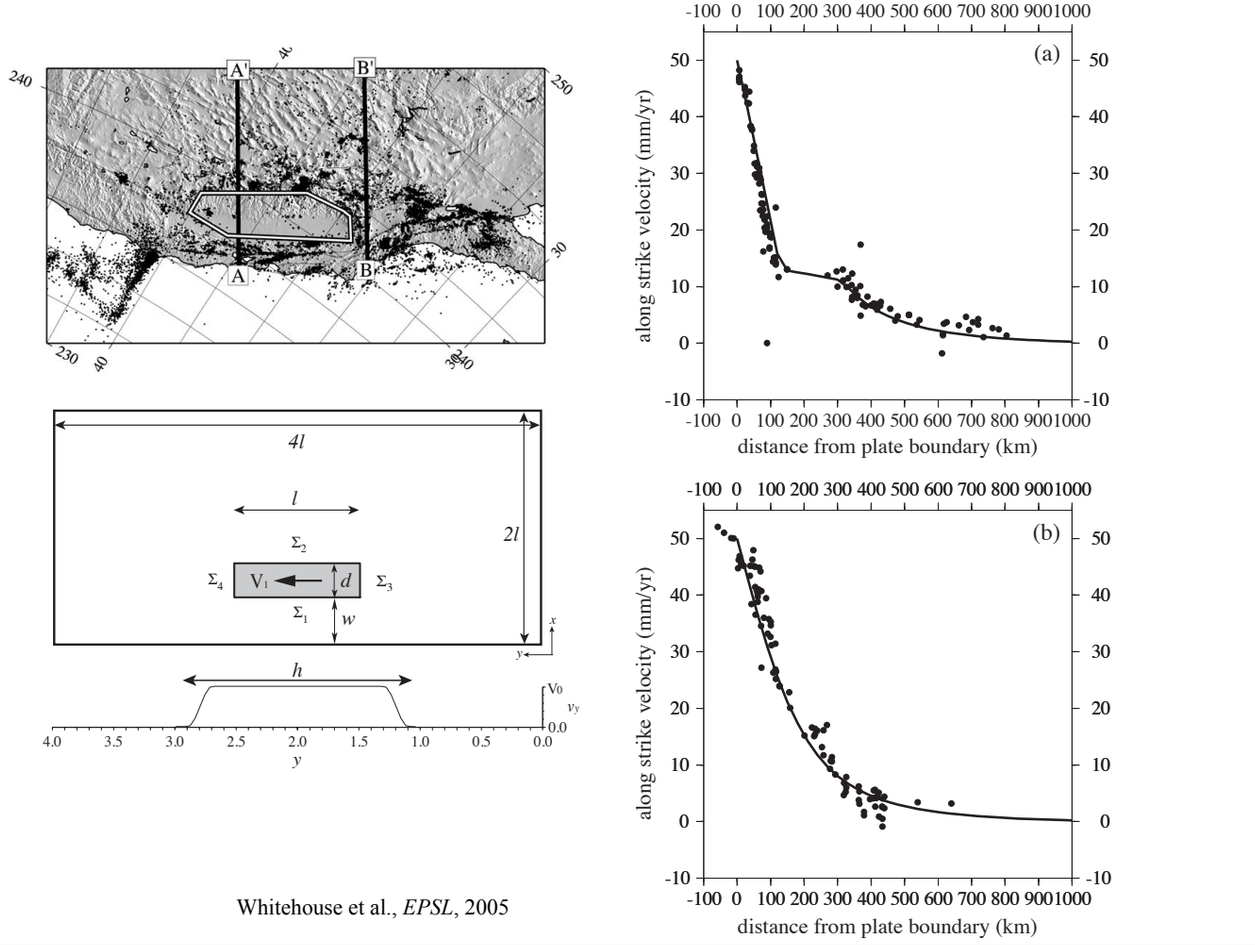

Whitehouse et al., *EPSL*, 2005

Can this help us understand what is going on? One interpretation is that the distributed shear is simply the response of a rigid block in an otherwise uniformly deforming medium. On right, dots are GPS observations, lines from the model

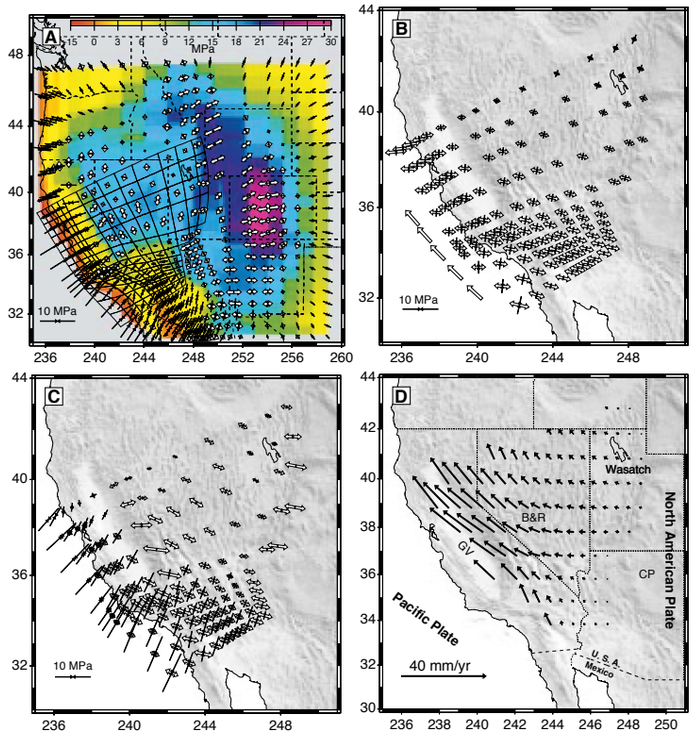

Fig. 2. (**A**) The minimal root mean squared deviatoric stress field determined from GPE variations, calculated assuming Airy compensation of topography. Different colors represent Δ GPE values $\bar{\sigma}_{zz}$ relative to a column of lithosphere at sea level. Tensional stress is shown as open white principal axes, and compressional stress is shown as black principal axes. (**B**) Stress field boundary conditions. The analog motion (open arrows) associated with these boundary conditions has a PA-NA pole that is ~10° west of the NUVEL-1A (*4*) PA-NA pole. (**C**) The total vertically averaged (over L = 100 km) deviatoric stress field, that is, the sum of stresses due to potential energy variations (A) and plate interaction (B). (**D**) The self-consistent flow field determined from strain rates calculated by scaling the total stress tensor field (C) by the inverse of viscosity (Fig. 4) for all areas east of the San Andreas fault (*32*).

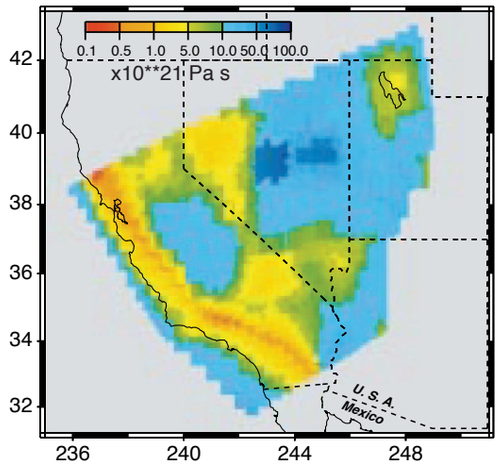

Fig. 4. The vertically averaged effective viscosity (over L = 100 km) for the western United States determined by dividing the magnitude of the total deviatoric stress (Fig. 2C) by the magnitude of the strain rate (*2*) for each grid area determined from the self-consistent kinematic model (Fig. 1).

Flesch et al., Science, 2000

What can we do with this dense data at an even broader scale? In a Newtonian fluid, strain rate is proportional to stress--if we can estimate it from GPE and boundary conditions, can make an estimate of strength [there are a number of problems in this application, but a useful illustration].

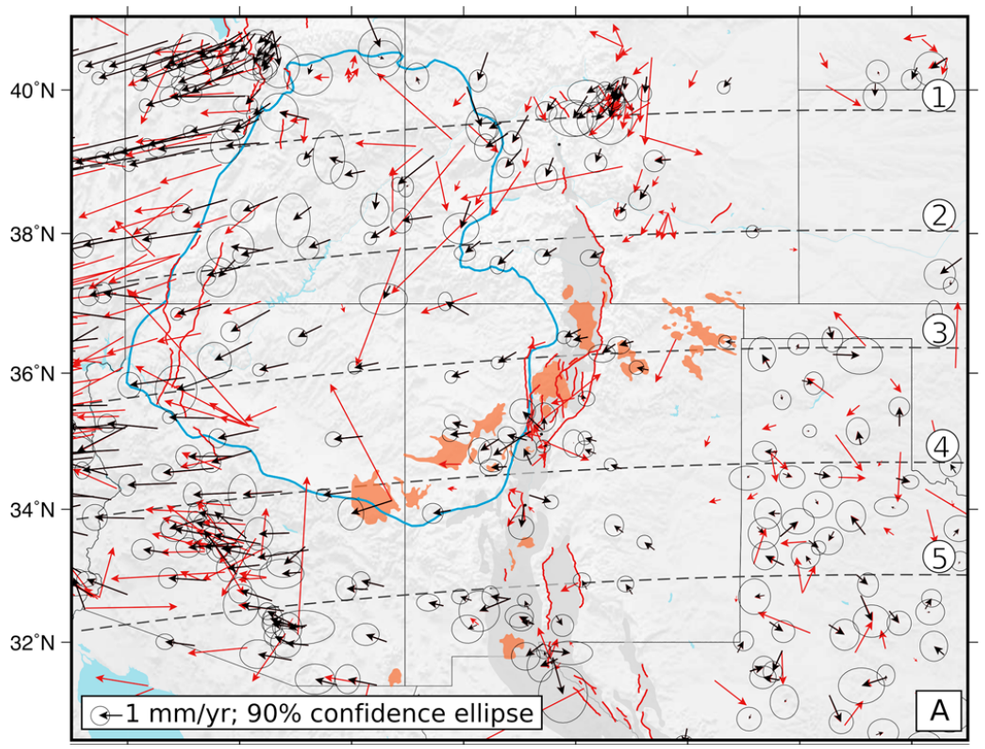

Murray et al., *JGR*, 2019

And there remain surprises yet in the data—this is crossing the “stable” Colorado Plateau

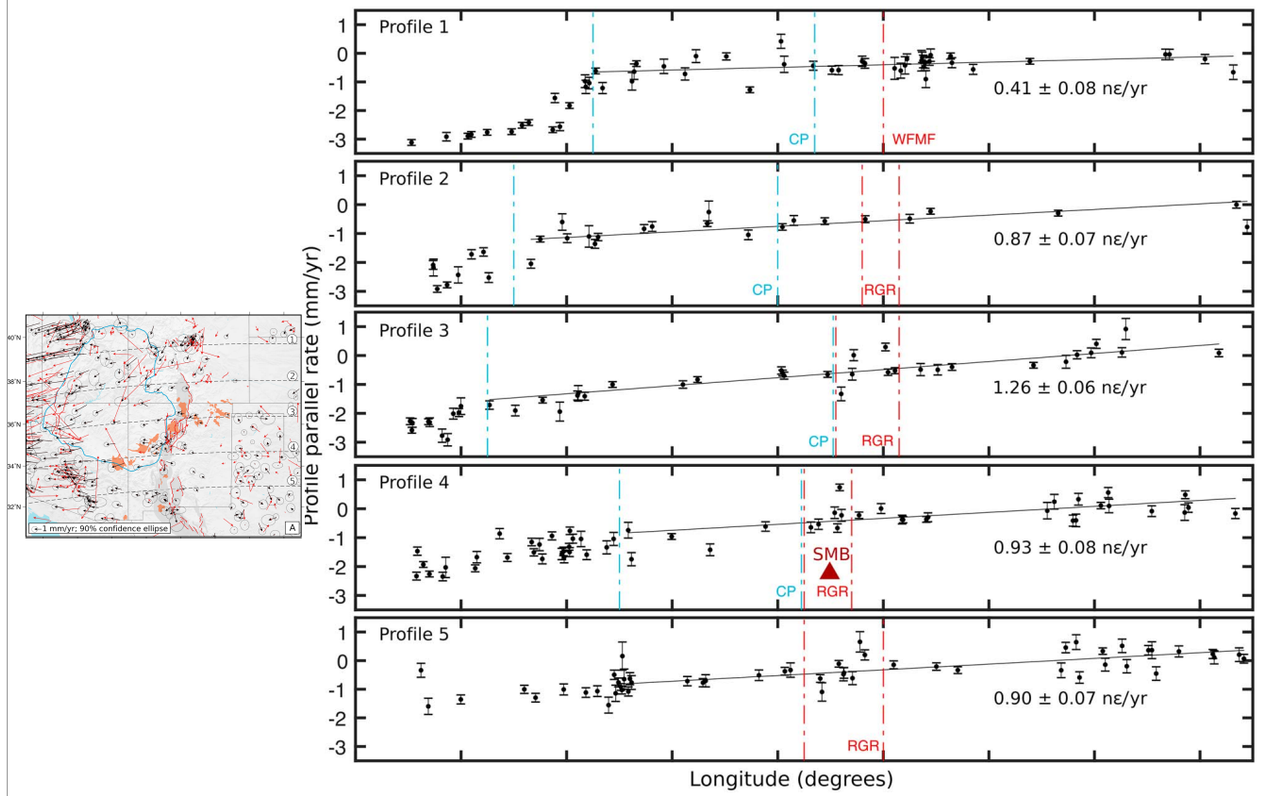

Murray et al., *JGR*, 2019

And there remain surprises yet in the data--for instance, how is this possible? No sign of loading near Rio Grande Rift, but finite strain rates going across a lot of the Colorado Plateau. SMB = Socorro Magma Body.

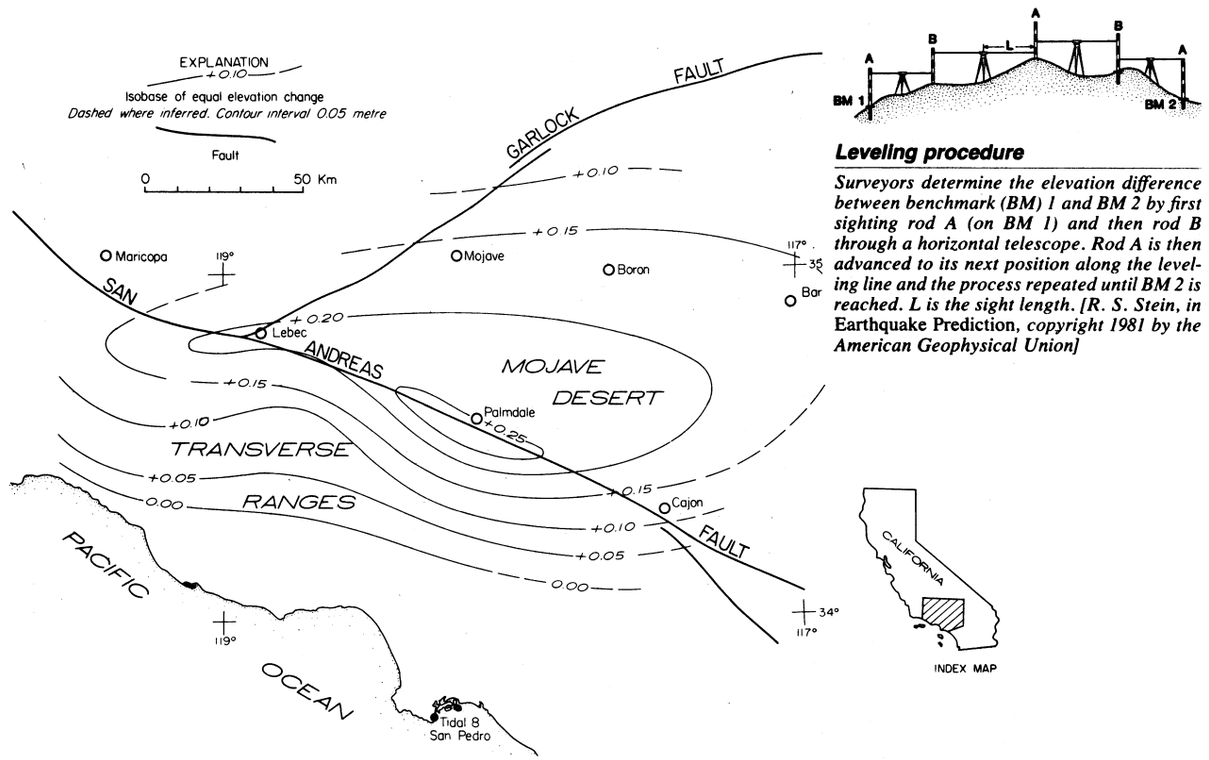

Fig. 1. Minimum uplift in the Transverse Ranges and adjacent parts of the Mojave Desert, California, during the period 1959–74.

Castle et al., 1976

OK, move on to vertical. Palmdale bulge story--real or not?

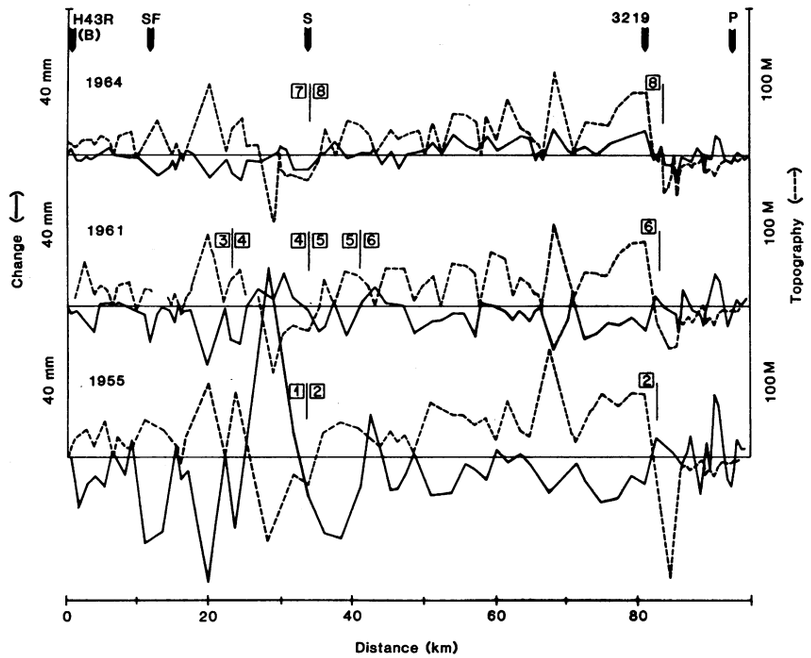

Fig. 1. Topography (dashed lines) and apparent change from 1965 (solid lines) for the profile from Burbank (*B*) to San Fernando (*SF*) to Saugus (*S*) to Palmdale (*P*). Topography and change are defined in Eqs. 1 and 2, respectively. Boxed numerals designate segments referred to in Table 1. Note the reversal of correlation between change and topography at Saugus in 1964. The topography differs slightly from year to year because of differences in bench marks used.

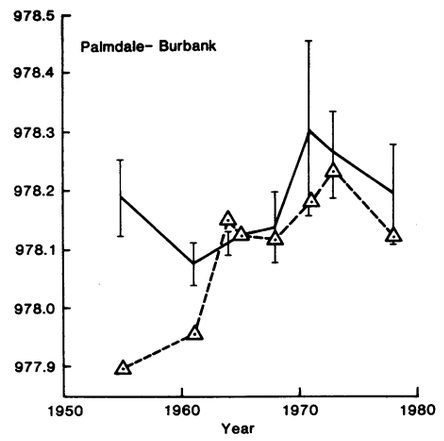

Fig. 2. Elevation difference in meters between bench marks 3219 (Palmdale) and H43R (Burbank) versus time. The dashed line is derived from data supplied by the National Geodetic Survey (*12*), with standard correlation for rod errors. The solid line shows the result of applying empirical correction based on correlation between apparent change and topography of short wavelength features. The errors bars for the corrected data represent 1 standard deviation, as computed with Eq. 5.

The change at Saugus (S) in 1964 suggests a problem with equipment—change relative to 1965 (solid line) correlates at short wavelengths with difference in topography (next benchmark elevation – benchmark elevation).

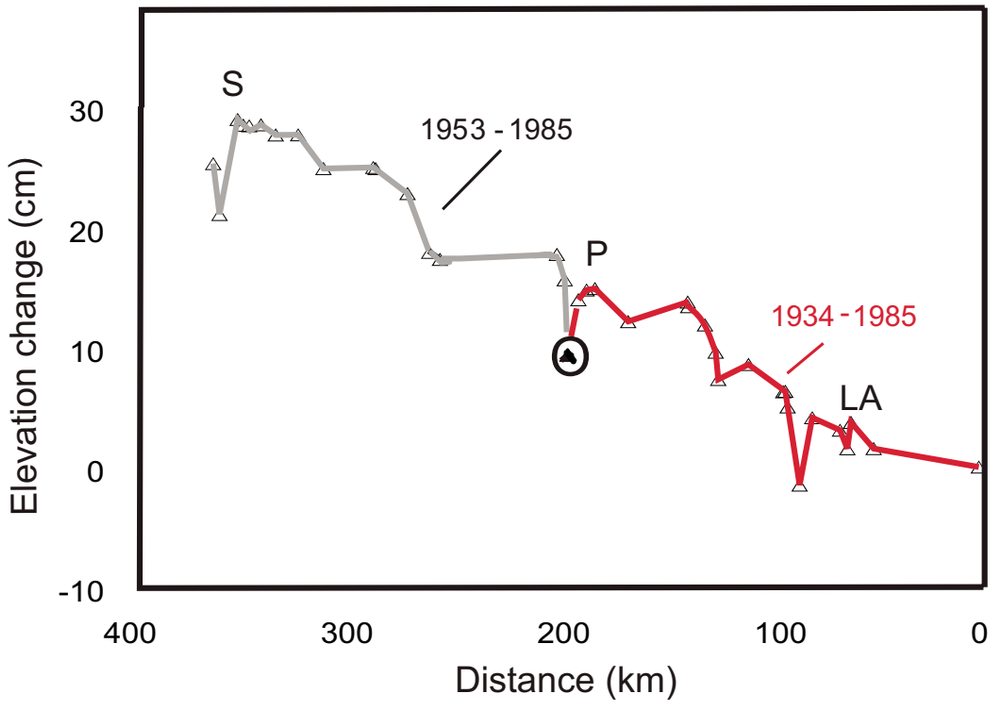

Figure 13. Profile of elevation changes along U.S. Highway 50 from an arbitrary starting point east of the town of Las Animas, Colorado, on the Great Plains, as determined from first-order leveling and re-leveling. The line continues westward to Salida, Colorado, in the mountains. Towns: S—Salida; P—Pueblo; LA—Las Animas.

Eaton, Geosphere, 2008

And yet the lessons have not been well learned...Count the problems here...but if taken literally would imply an uplift rate of 30 cm over 50 years (at most) or 6 mm/yr = 6 km/My, which would be one of the highest rates in the world and would produce the modern Rockies in half a million years

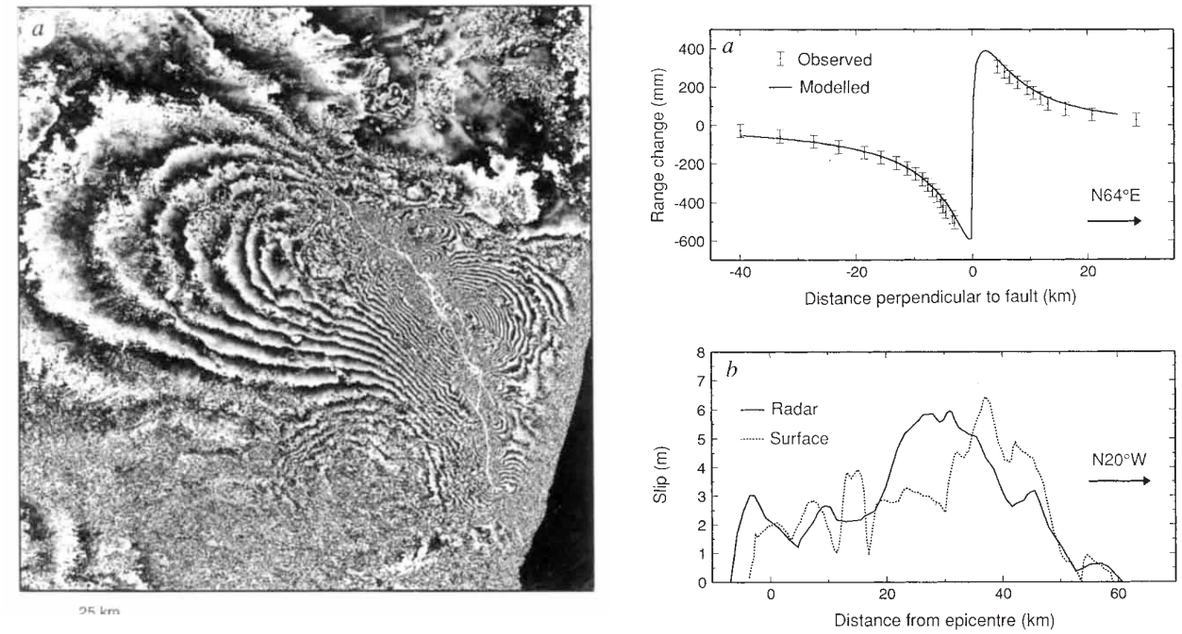

Massonnet, Nature, 1993

InSAR's big splash was the 1992 Landers earthquake (which rather quickly supported the geodetic inferences of Sauber et al.). So clear earthquake-source and afterslip tool...

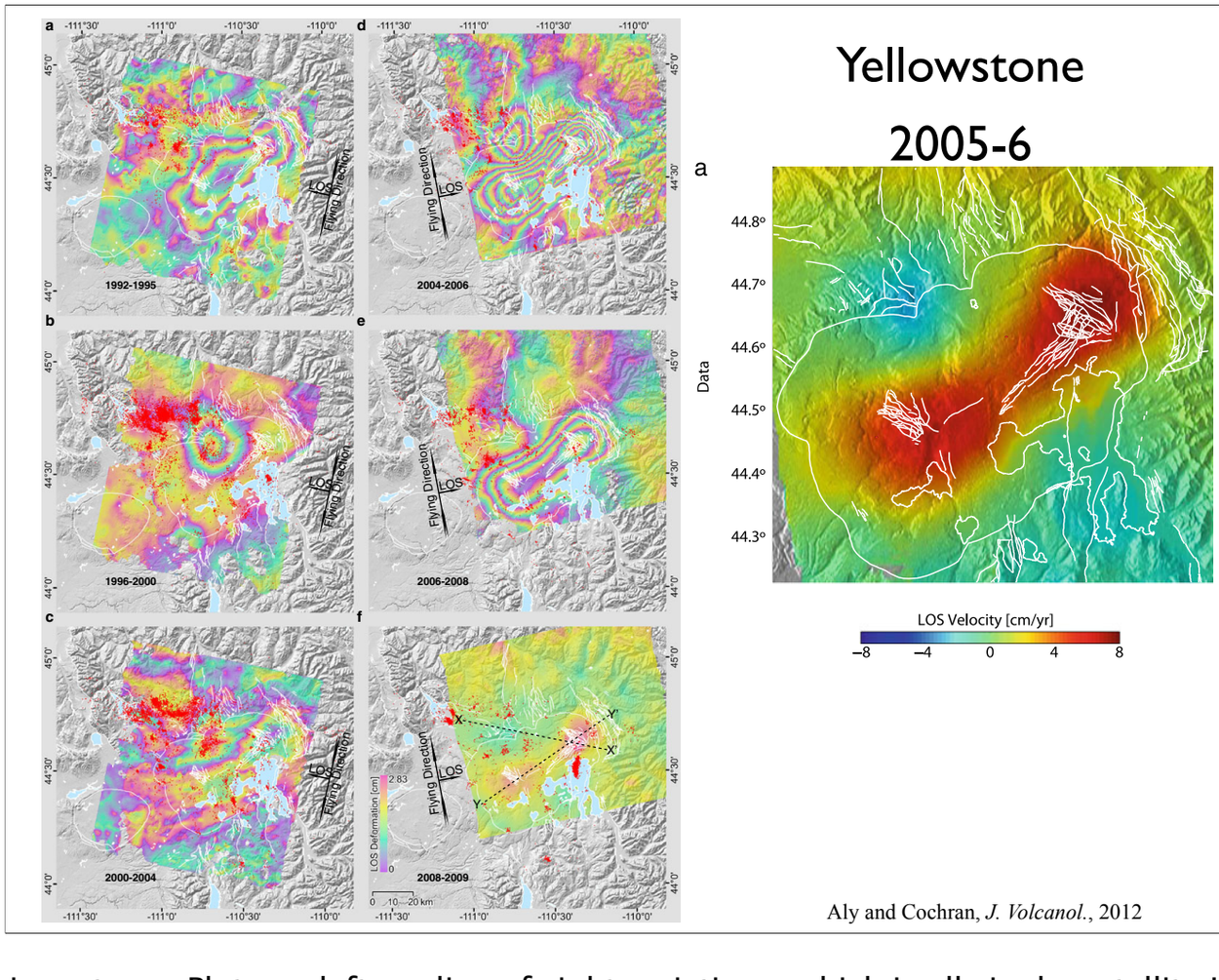

Aly and Cochran, *J. Volcanol.*, 2012

…which can also be applied to volcanic systems. Plots on left are line of sight variations, which is all single-satellite InSAR can give. Note that careful examination of fringes shows things going up and down...

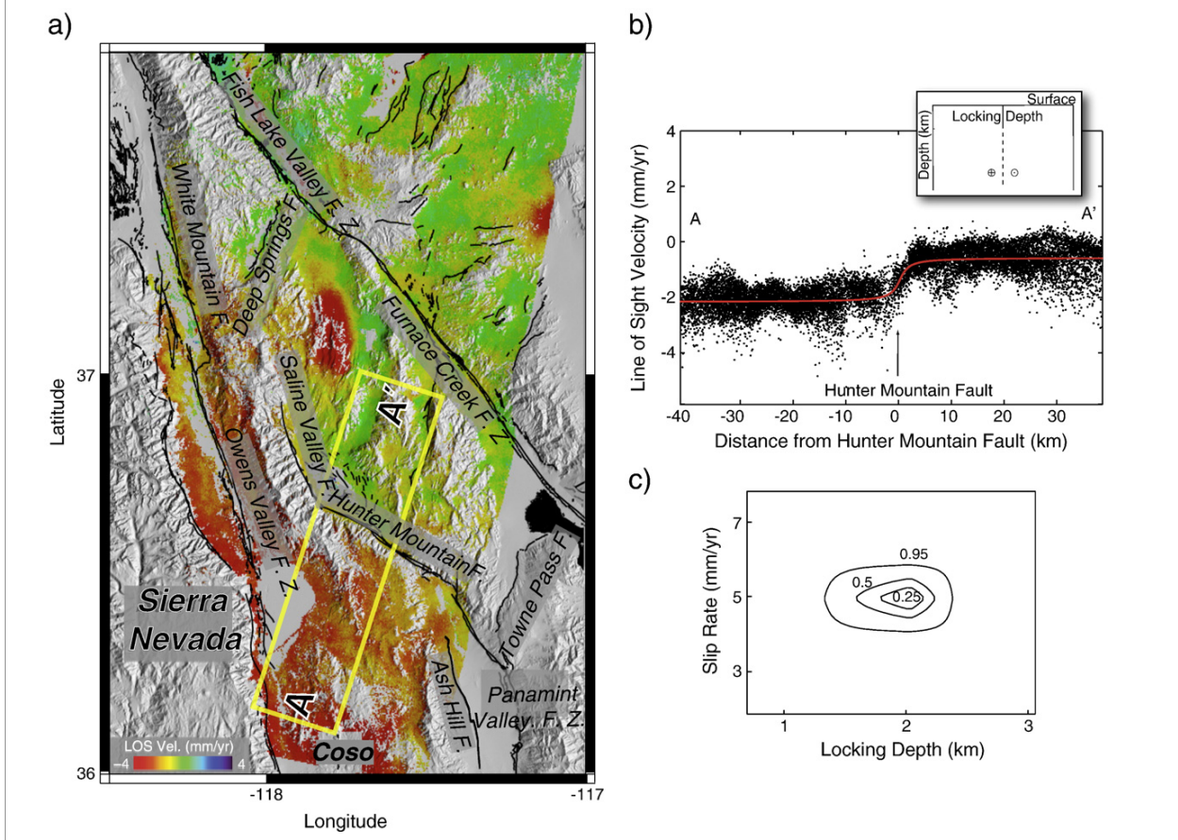

Gourmelen et al., *EPSL*, 2011

Rather more unusual use--constrain locking depth and slip rate of a fault without an earthquake. I cannot find what the line of sight is here. Fig. 3. InSAR surface displacement map and fault slip rate modeling for the Hunter Mountain fault (modified from Gourmelen et al. (2010)) a) InSAR based Line of Sight (LOS) velocity map for the ECSZ, based on data acquired between 1992 and 2000. Red oval marks coseismic plus post-seismic displacement associated with the 1993 M 6.1 Eureka Valley earthquake (Peltzer and Rosen, 1995). Yellow box shows location of profile in Figure 3b. F is Fault, FZ is Fault Zone. Faults are from the USGS quaternary fault database (U.S. Geological Survey, New Mexico Bureau of Mines and Mineral Resources and Nevada Bureau of Mines and Geology, 2006). b) Line Of Sight displacement along A–A′ (Fig. 3a). Strain accumulation model in red, assuming a vertical fault, with locked (solid line) and freely slipping (dashed line) segments (inset). Note high strain rate near fault, corresponding to shallow locking depth. Best-fit slip rate is 4.9 ± 0.8 mm/yr assuming pure strike slip in the strike direction of Hunter Mountain Fault. c) Model parameters (Brooks and Frazer, 2005), for the model in Figure 3b showing tradeoff between slip rate and locking depth. Unlike models with deeper locking depth, there is little tradeoff between slip rate and locking depth.

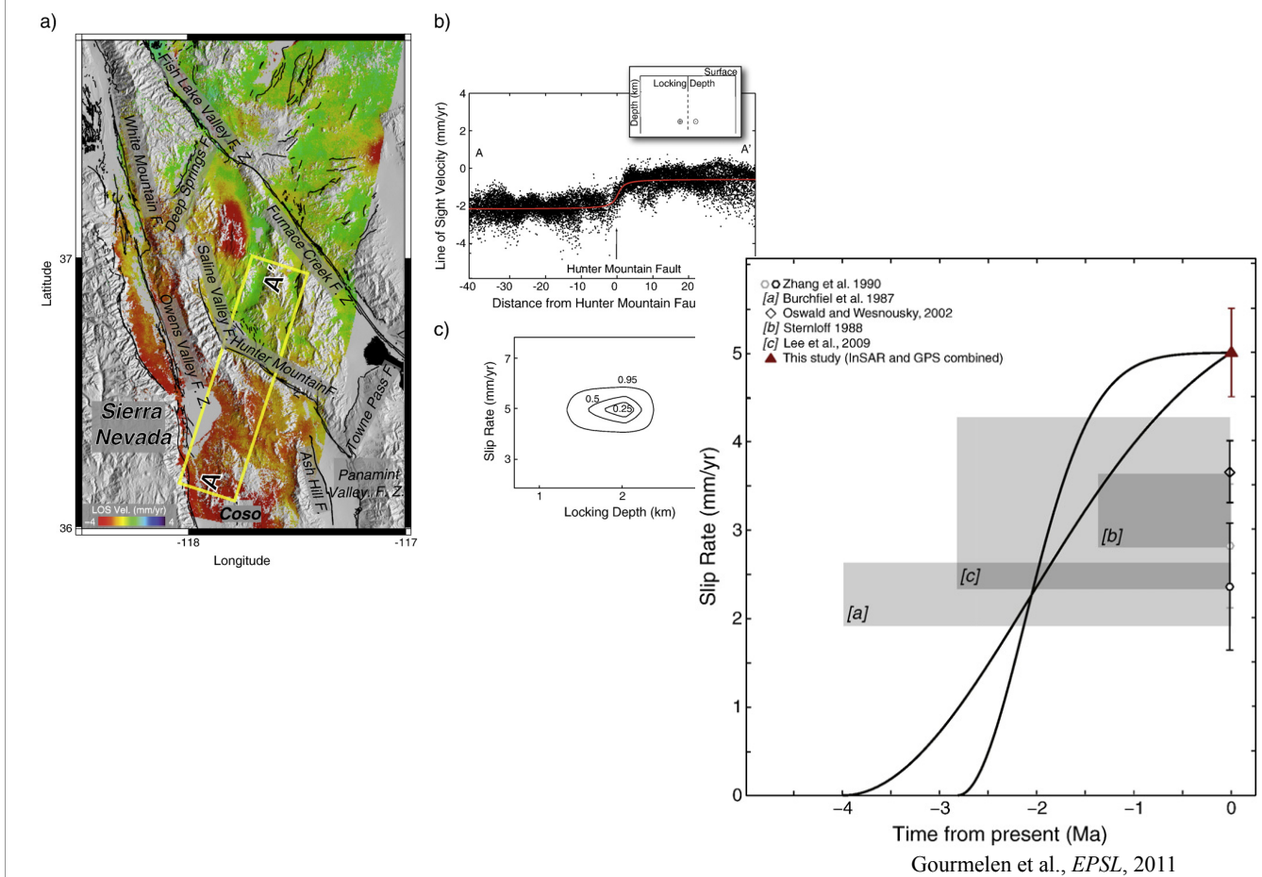

Gourmelen et al., *EPSL*, 2011

Slip rate inferred here is higher than neotectonic rates--these kinds of discrepancies in rates vs geodesy are a common issue in B&R [could add more--Owens Valley fault is a prime example]

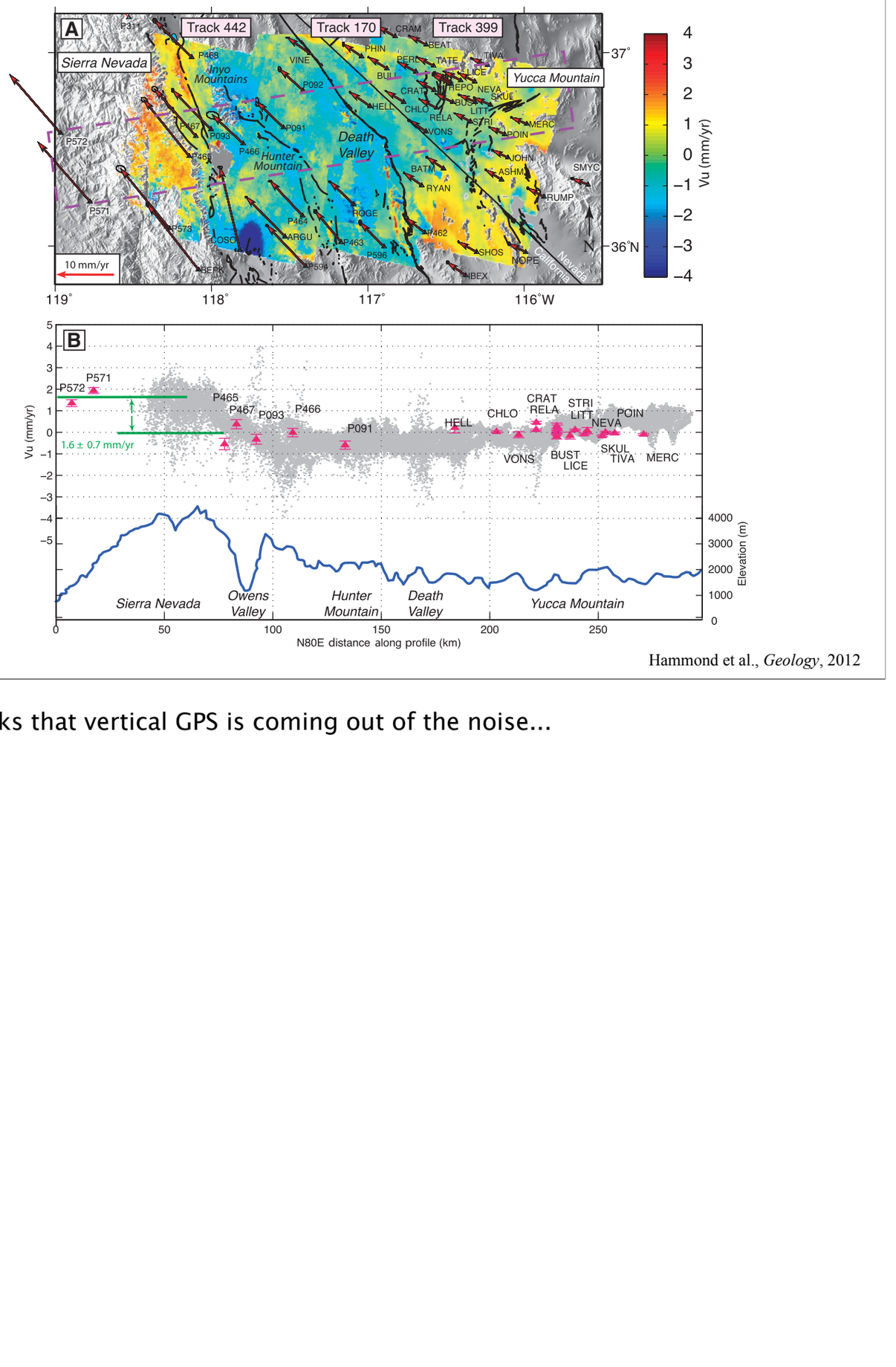

Hammond et al., *Geology*, 2012

Combining InSAR and GPS, this paper thinks that vertical GPS is coming out of the noise...

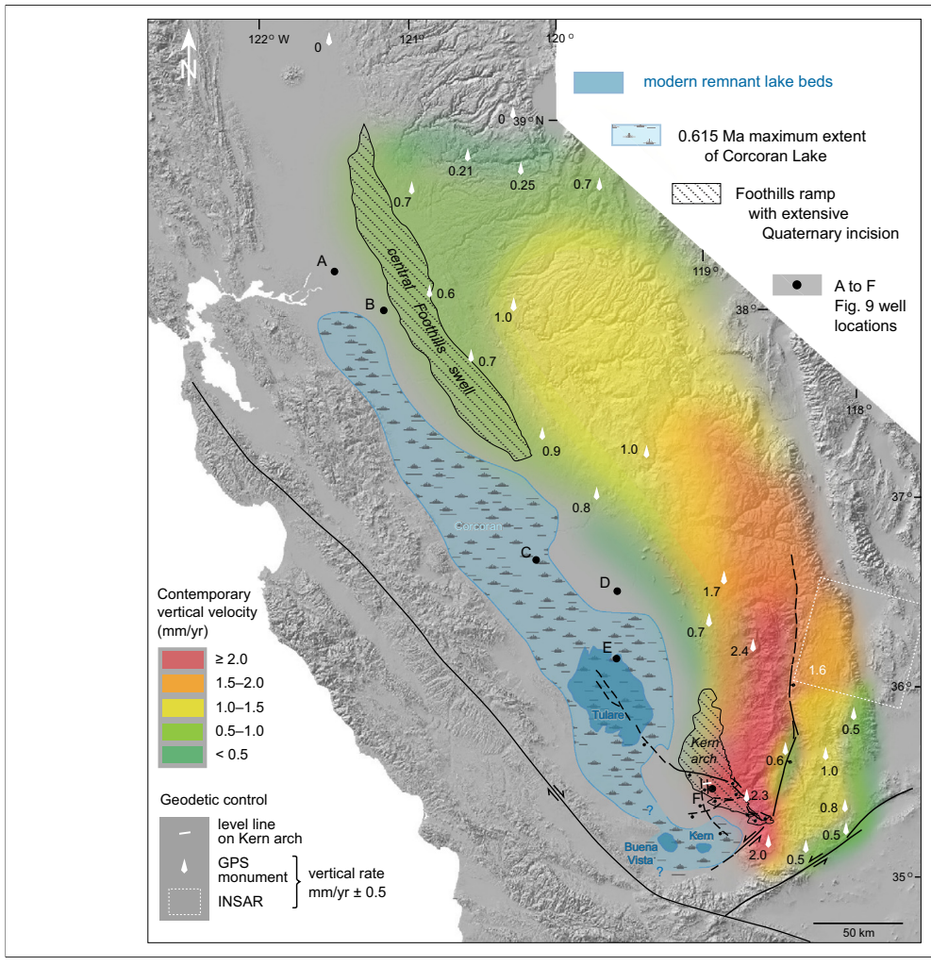

Saleeby et al, *Geosphere*, 2013

Vertical GPS accepted and interpreted by Saleeby et al in Sierra...

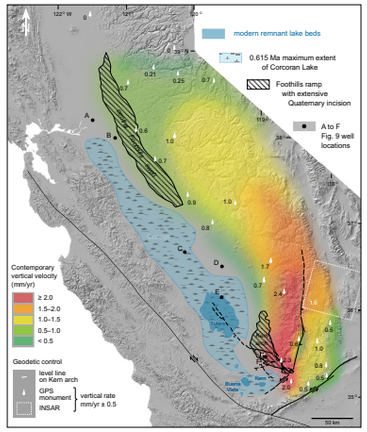

Saleeby et al, *Geosphere*, 2013

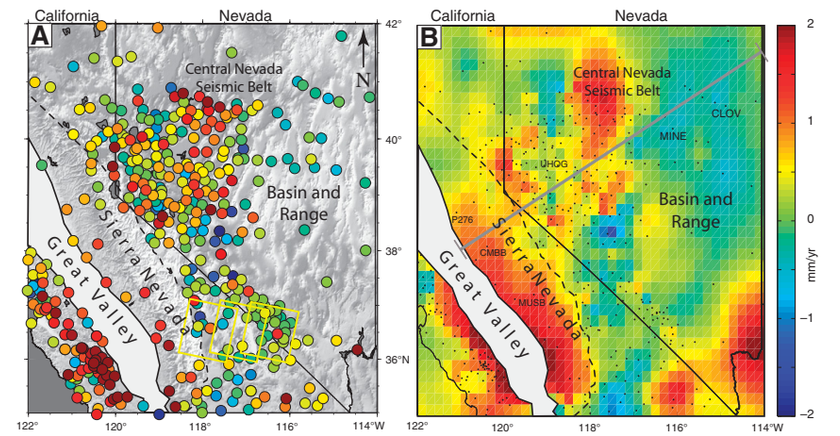

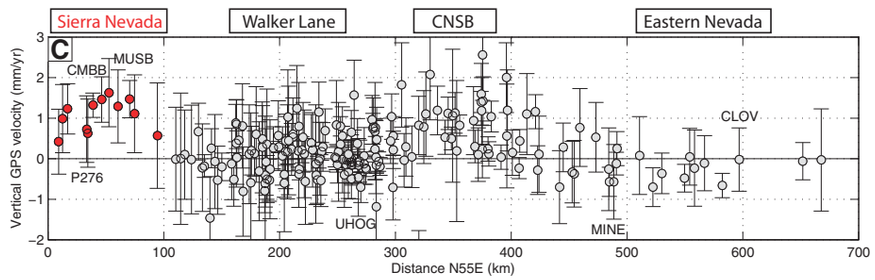

Hammond et al., *Geology*, 2012

Vertical GPS accepted and interpreted by Saleeby et al in Sierra...just keep in mind it is a noisy dataset. Notice though how uplift seems to be focused on the edge of the Great Valley…

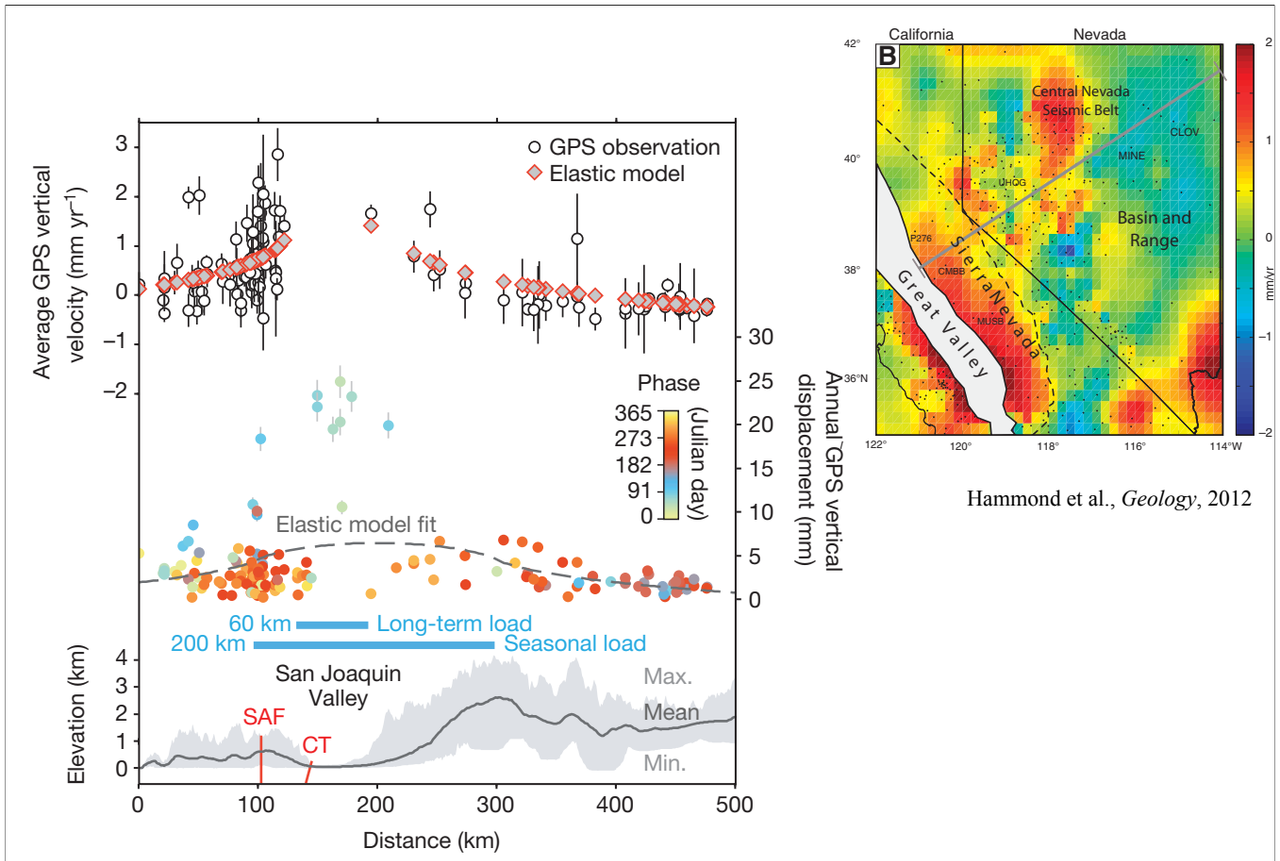

Amos et al., *Nature*, 2014

Hammond et al., *Geology*, 2012

Amos et al. argue that this is actually from groundwater withdrawal in the Great Valley. Argue that seasonal changes in vertical due to summer withdrawals in the GV (long-term load) and snow+rain in winter months in mountains (seasonal load). [Which is mostly fine, but that elastic model is a problem: it is a half space model with no true zero].

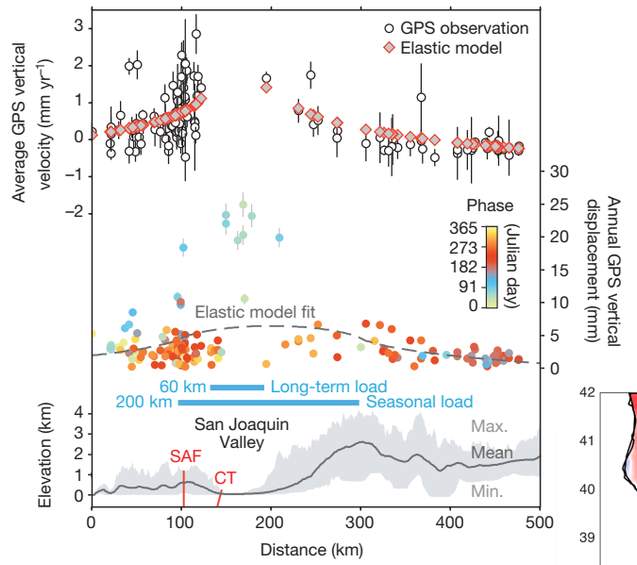

Amos et al., *Nature*, 2014

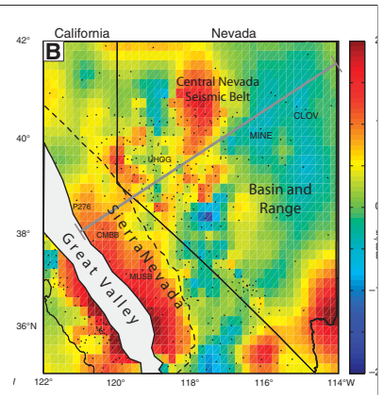

logy, 2012

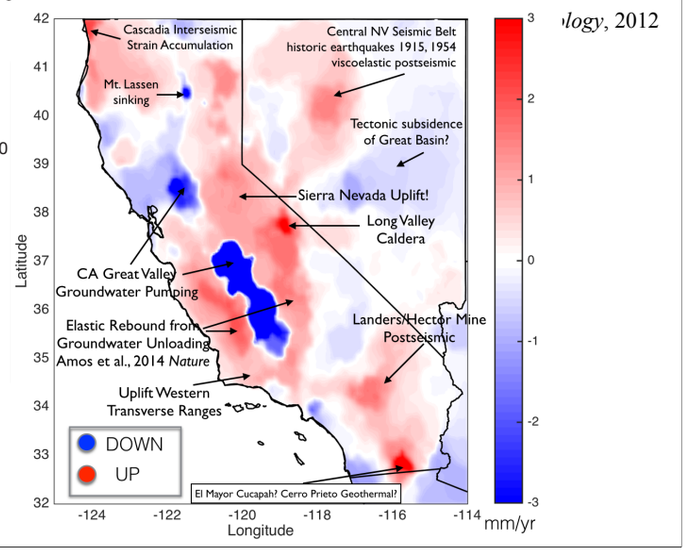

Hammond et al., *Fall AGU*, 2015

Hammond et al. incorporate that but still like some uplift in Sierra (nearly the same as in their 2016 paper in JGR, but this figure's annotations are helpful)

Vertical displacements over time

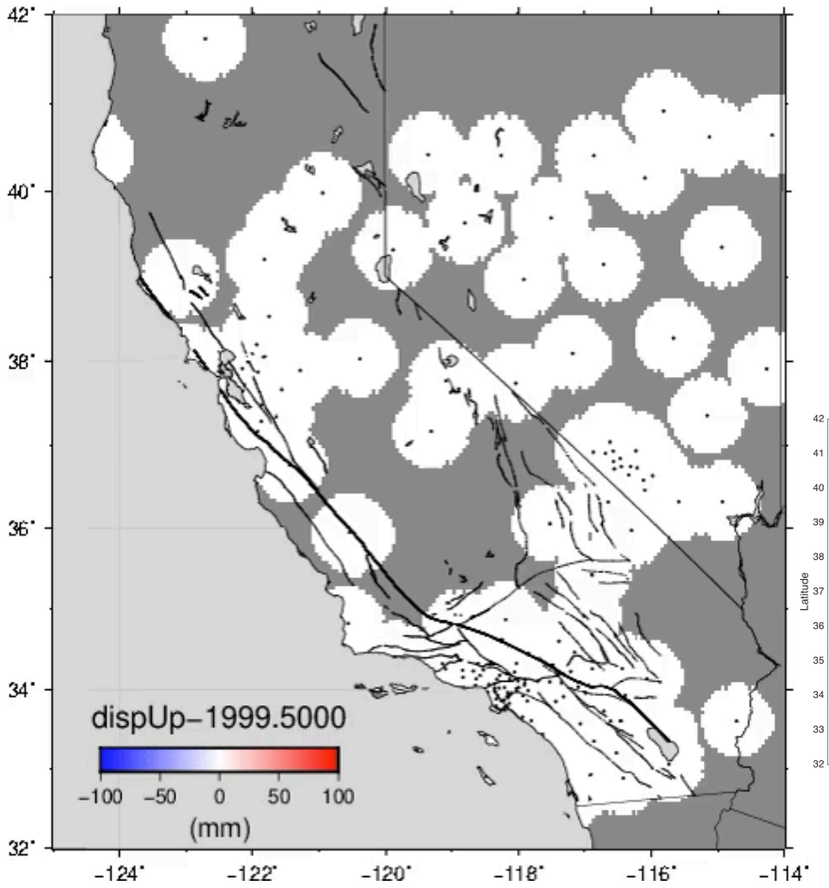

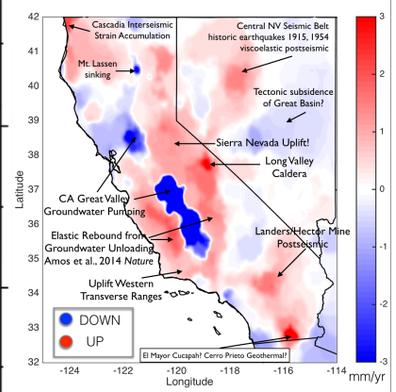

Klein et al., JGR, 2019

Animated vertical GPS kind of highlights how unstable it can seem to be.

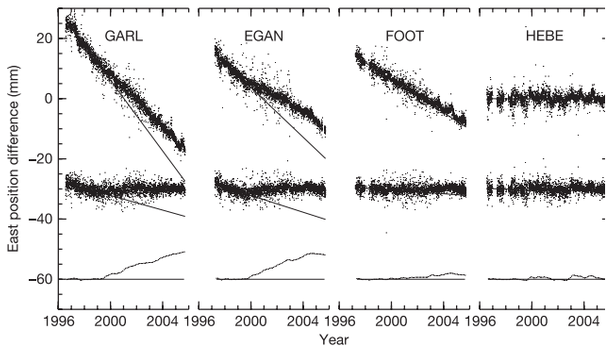

Figure 2 | Illustration of the post-analysis procedure, using time series o east position for four BARGEN sites. Top, 'raw' time series, in a North America-fixed geodetic reference frame (see Methods). Error bars are omitted for clarity, but are generally ~1 mm. The straight line is the best-fi straight line using position estimates from the first 2.5 years. Middle, residuals of the raw time series from a best-fit model consisting of a straigh line and seasonal (annual and semi-annual sinusoids) terms. A statistical approach that allowed these terms to change with time in a constrained manner was used (see Methods). Bottom, residuals smoothed with a gaussian filter with a full-width at half-maximum (FWHM) of ~8 months. A model based on a linear fit to the first 2.5 years of data has been removed. The evolution of these final time series thus indicates deviation from temporally linear motion.

Davis et al., Nature, 2006

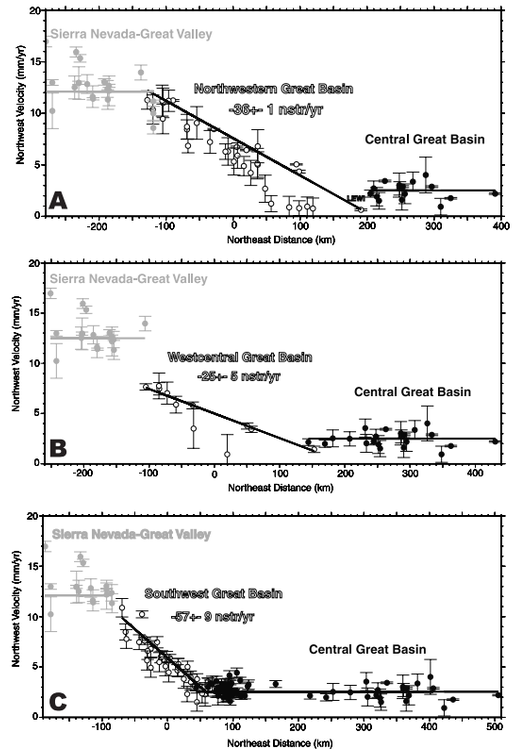

Figure 14. (a) N37°W components of velocity as a function of N53°E distance for the Sierra Nevada–Great Valley (SNGV; gray circles), northwestern Great Basin (NWGB; open circles), and central Great Basin (CGB; solid circles) domains. Velocities refer to the North America reference frame. Error bars represent 1 standard deviation. Both data and model have been corrected using equations (2) and (3). The lines show the block-strain model. Zero slope indicates that the SNGV and CGB regions are not internally deforming in the model. Site LEWICGPS in the northwest Great Basin domain is labeled. (b) Same as for Figure 14a but for west central Great Basin domain (CWGB). (c) Same as for Figure 14a but for southwestern Great Basin domain (SWGB).

Bennett et al., Tectonics, 2003

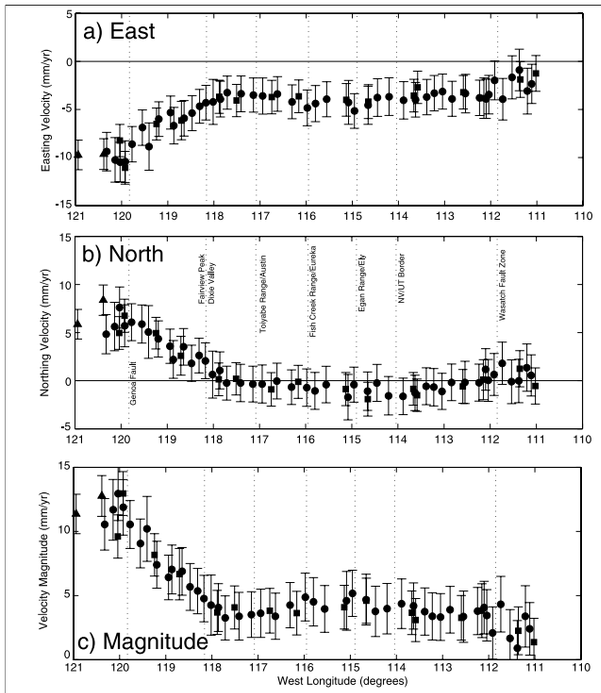

Figure 2. (a) East component, (b) north component, and (c) magnitude of velocity with respect to North America. The error bars indicate 2σ uncertainty. Vertical dotted lines show longitude of the indicated fault or geographic feature, squares are off-axis sites, circles are on-axis sites, and triangles are the sites QUIN (near 121°W) and CMBB (near 120.5°W) on the SNGV. (d) Relative plate motion normal component $V_{\perp}$, i.e., component of GPS velocity that lies along the great circle between the Pacific–North America pole of rotation and the GPS site, positive to the northeast, (e) relative plate motion parallel component $V_{//}$, i.e., the horizontal component tangent to the small circle around the pole, positive northwest, and (f) geographic azimuth of velocity, measured as degrees clockwise from north. Horizontal axis is distance from the center of the network projected along the great circle connecting the Pacific–North America pole and the center of the network. Other symbols are as in the previous figure.

Hammond & Thatcher, JGR, 2004

Fig. 1. 1992–2000 LOS velocity map for the area of the 1915–1954 Nevada earthquakes together with epicenters (blank circles), focal mechanisms (spheres), and surface ruptures. Green arrows, campaign GPS velocities (7); red arrows, Basin and Range Geodetic Network (BARGEN) permanent GPS velocities and site names (9). LOS is velocity considered positive for decreasing distance between ground and satellite.

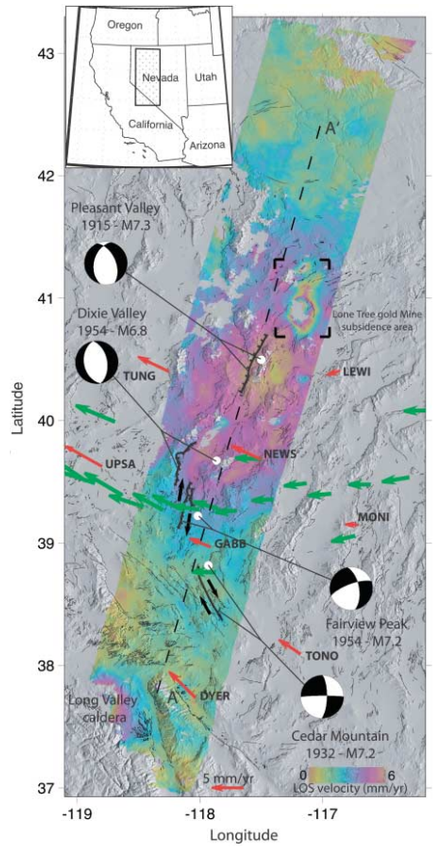

Gourmelon et al., Science, 2005

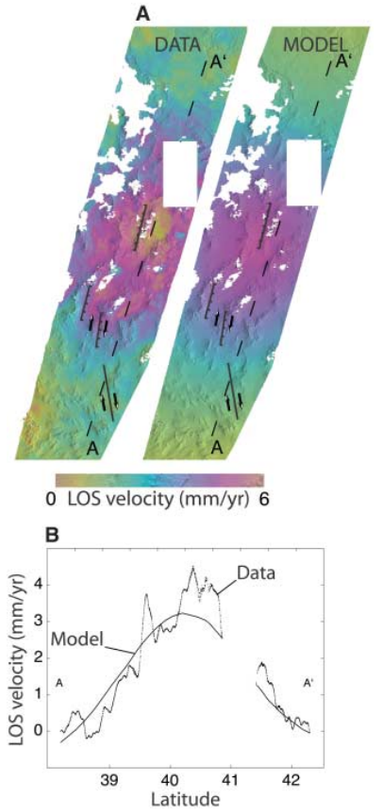

Fig. 4. (A) Data and best fitting postseismic relaxation model (Lone Tree gold mine deformation area has been masked out). (B) Profile [dashed lines in (A)].

Fig. 5. Bottom: Magnitude of horizontal campaign GPS velocities along an east-west profile through the Basin and Range (7). Upper line, measured velocities; lower line, measured velocities minus model-predicted postseismic deformation. Top: Simplified tectonic map of the Basin and Range. Triangles, locations of GPS stations; CNSB, Central Nevada Seismic Belt; WL, Walker Lane.

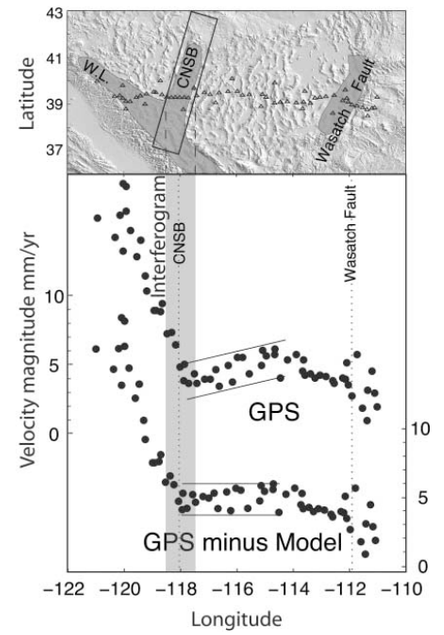

Gourmelon et al., Science, 2005

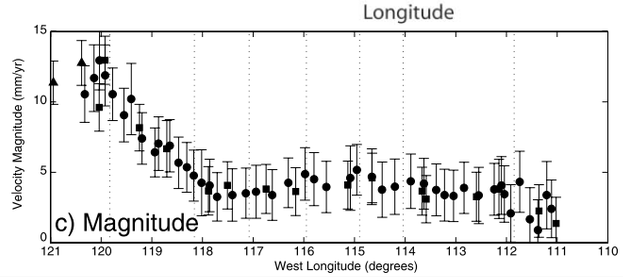

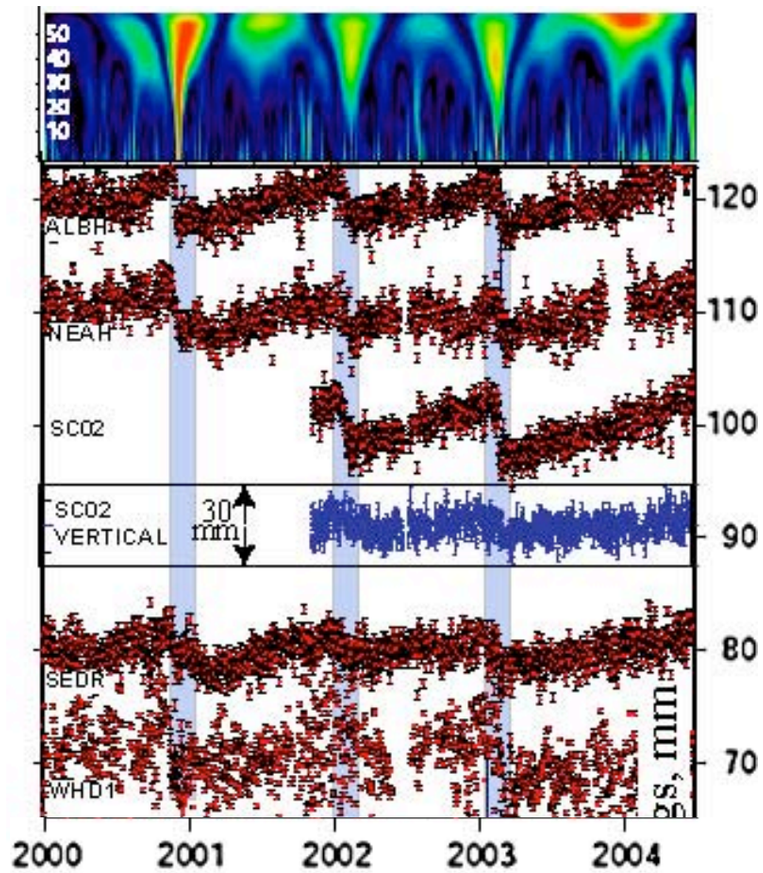

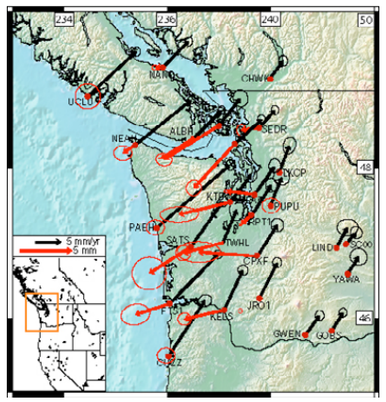

Figure 1. Slow earthquake displacements (red arrows) during the 2003 Cascadia event and interseismic deformation vectors (black) from continuous PANGA and WDCA GPS networks. 12 stations record discernible, transient reversals from NE-directed contraction to WSW-directed extension. The transient event emerged over seven weeks and spanned nearly 300 km along-strike, from the Oregon to Canadian borders of Washington State. Error ellipses are 1σ and variable size reflects time series scatter.

Melbourne et al.,GRL, 2005

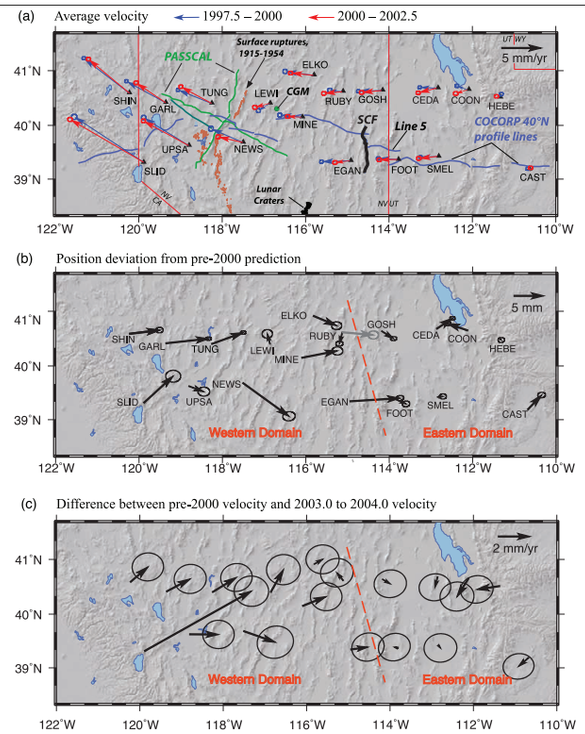

Figure 2. Map showing velocity and displacement fields associated with transient motions of the first 18 BARGEN sites installed across northern Great Basin, using the geodetic network solution of *Davis et al.* [2006]. (a) Average velocities for intervals 1997.5 to 2000.0 (blue arrows) and 2000.0 to 2002.5 (red arrows). Also shown are position of COCORP 40°N profile lines (blue), PASSCAL survey lines (green); traces of central Nevada seismic belt surface ruptures (brown) after *Bell et al.* [2004]; surface trace of Schell Creek fault (SCF); and the location of Cortez gold mine open pit operation (CGM). (b) Deviations from position predicted on the basis of pre-2000 site velocities [*Davis et al.* 2006], showing approximate boundary between eastern and western geodetic domains; deviations of sites CEDA and COON have been corrected for lake loading effects [*Elósegui et al.*, 2003] but likely still contain unmodeled hydrological signal from groundwater effects in the metropolitan area around Salt Lake City. Gray arrow for site RUBY shows deviation from pre-1998.5 estimated velocity. (c) Difference between 2003.0 to 2004.0 velocity and 1997.5 to 2000 average velocity (compare Figure 4 of *Davis et al.* [2006]).

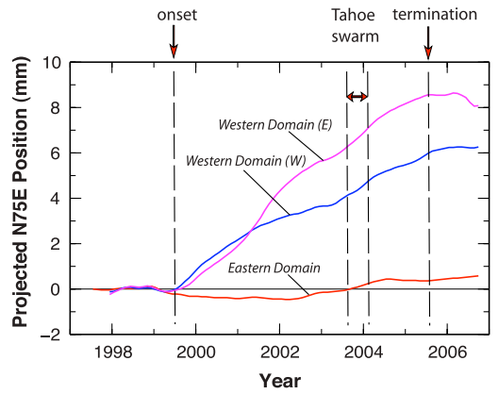

Figure 3. Regionally averaged (stacked) nonlinear deviations of N75°E position. Red indicates eastern domain sites (GOSH, FOOT, CAST, SMEL, COON, CEDA, HEBE, RUBY); purple indicates western domain sites ELKO, MINE, EGAN; blue indicates western domain sites NEWS, TUNG, UPSA, GARL, SHIN. Only data from a common epoch range (1997.9–2006.7) were used. The time series shown are an update of the time series in Figure 3c of *Davis et al.* [2006], using BARGEN data acquired through November 2006 and analyzed with the GAMIT/GLOBK analysis package version 10.3. The time series differ in that seasonal variation, previously modeled as sinusoidal amplitudes that varied in piecewise-continuous linear fashion, are here modeled as a continuously varying stochastic process and estimated using a Kalman filter.

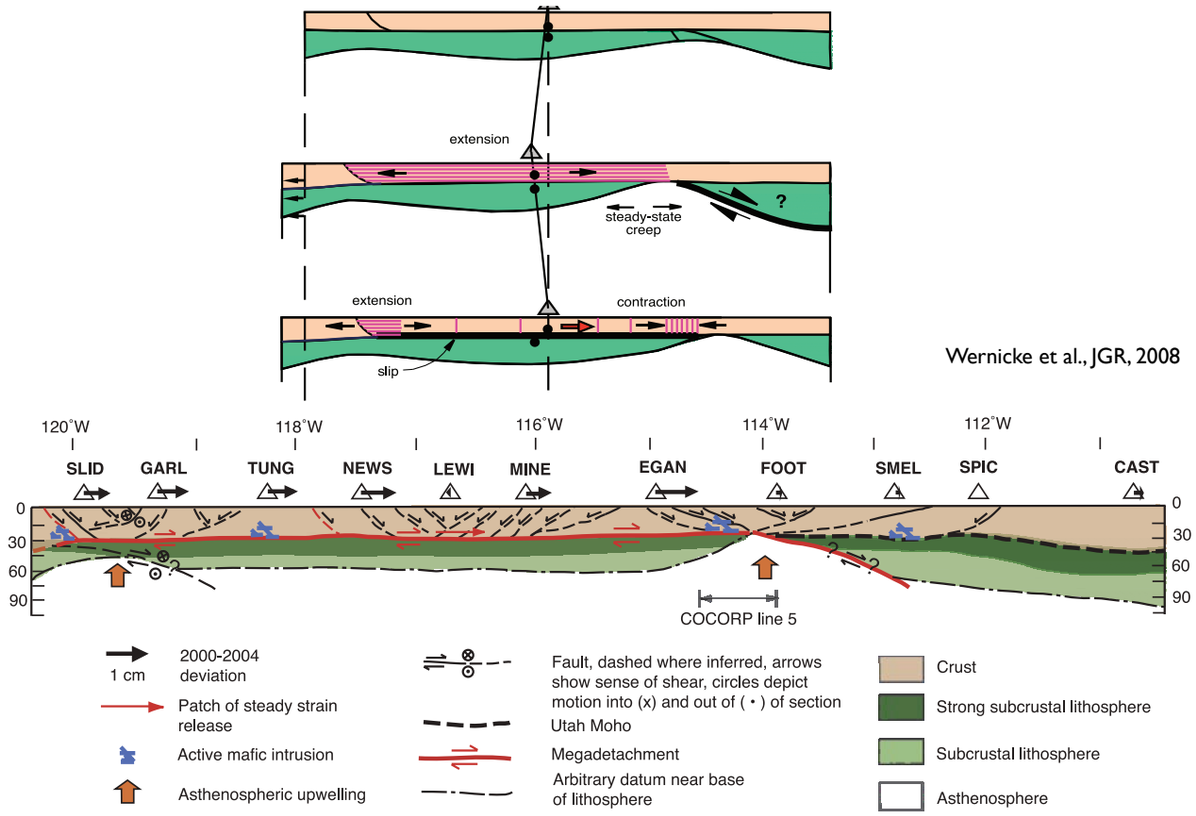

Figure 15. Cross-sectional tectonic model summarizing the primary function of the megadetachment and its relationship to active structures in the upper crust and inferred structures in the upper mantle. Section is constructed using interpretations along the COCORP 40°N profile (Figure 1) and data discussed in text.

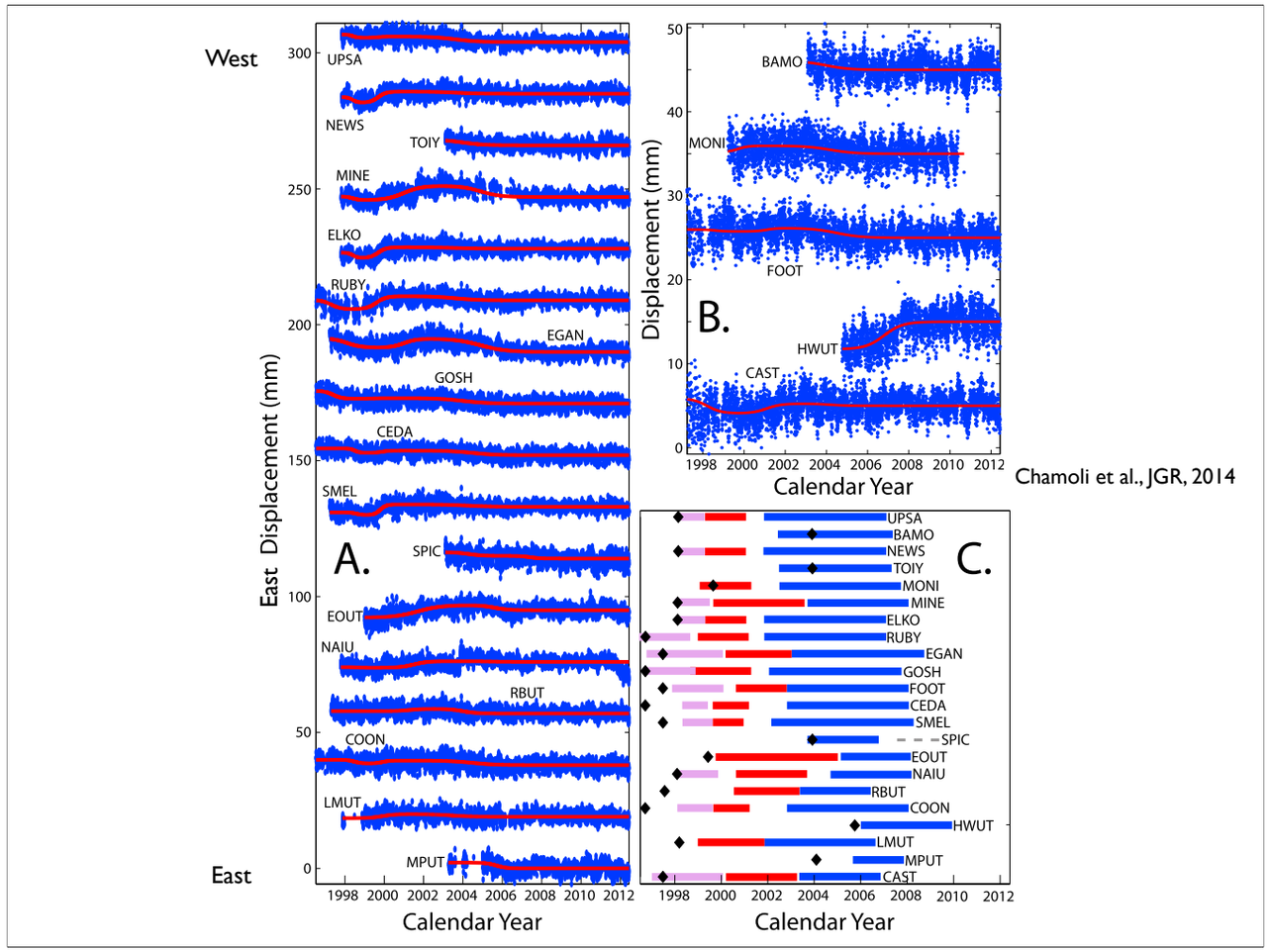

Chamoli et al., JGR, 2014

Longer time series suggests that the base case used by Wernicke et al. was actually anomalous. Displacement curves have had the background model derived from 2007–2012 removed; these authors identify unusual events in 1998, 2000, and 2004. These are most evident to the west; these all had northward motion as well.

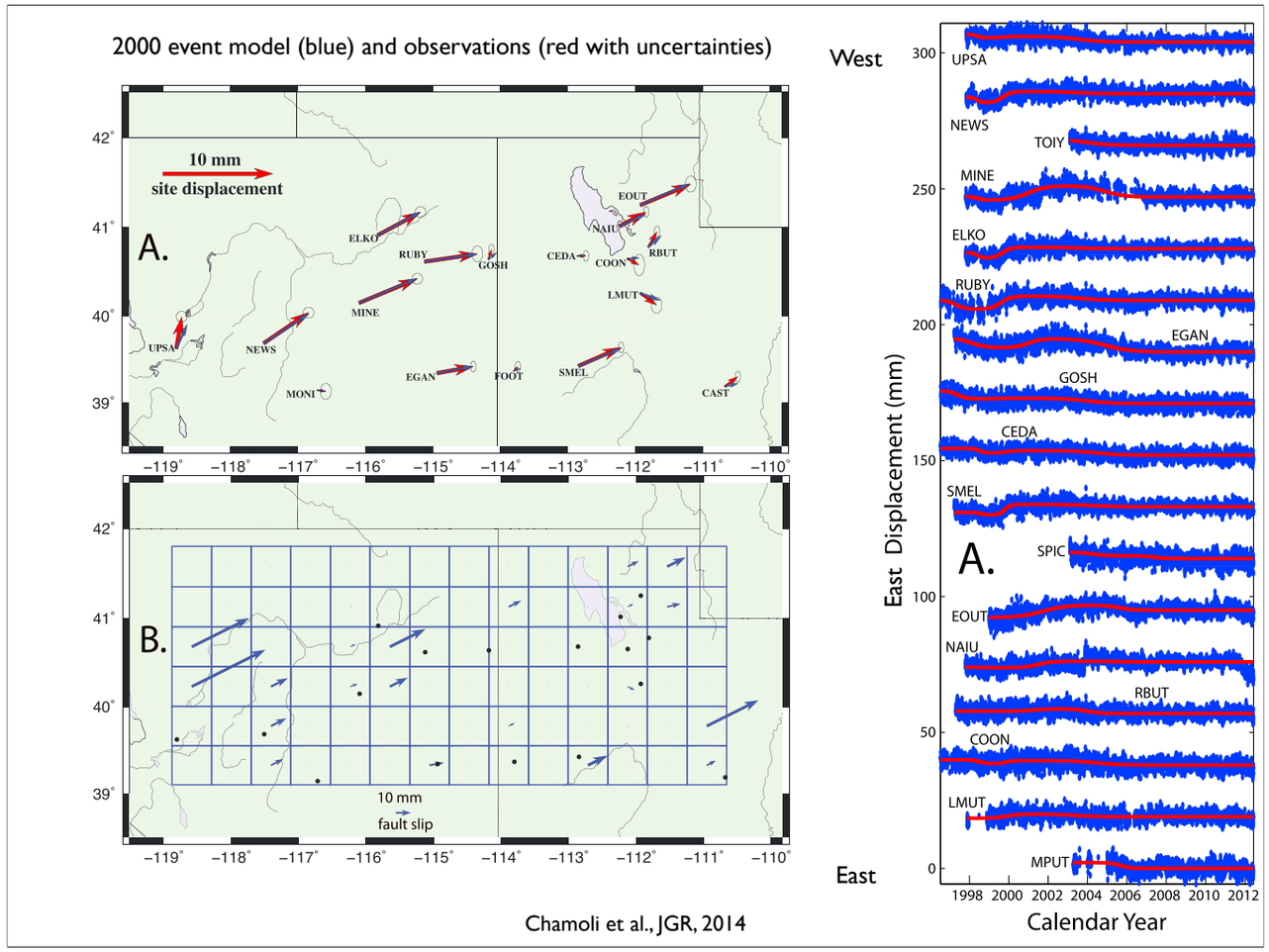

Chamoli et al., JGR, 2014

Modeling this suggests more localized displacement on fairly shallow structures; authors allow that this does still resemble the kind of episodic motions seen in Cascadia but prefer slip on LANFs as doing things here (

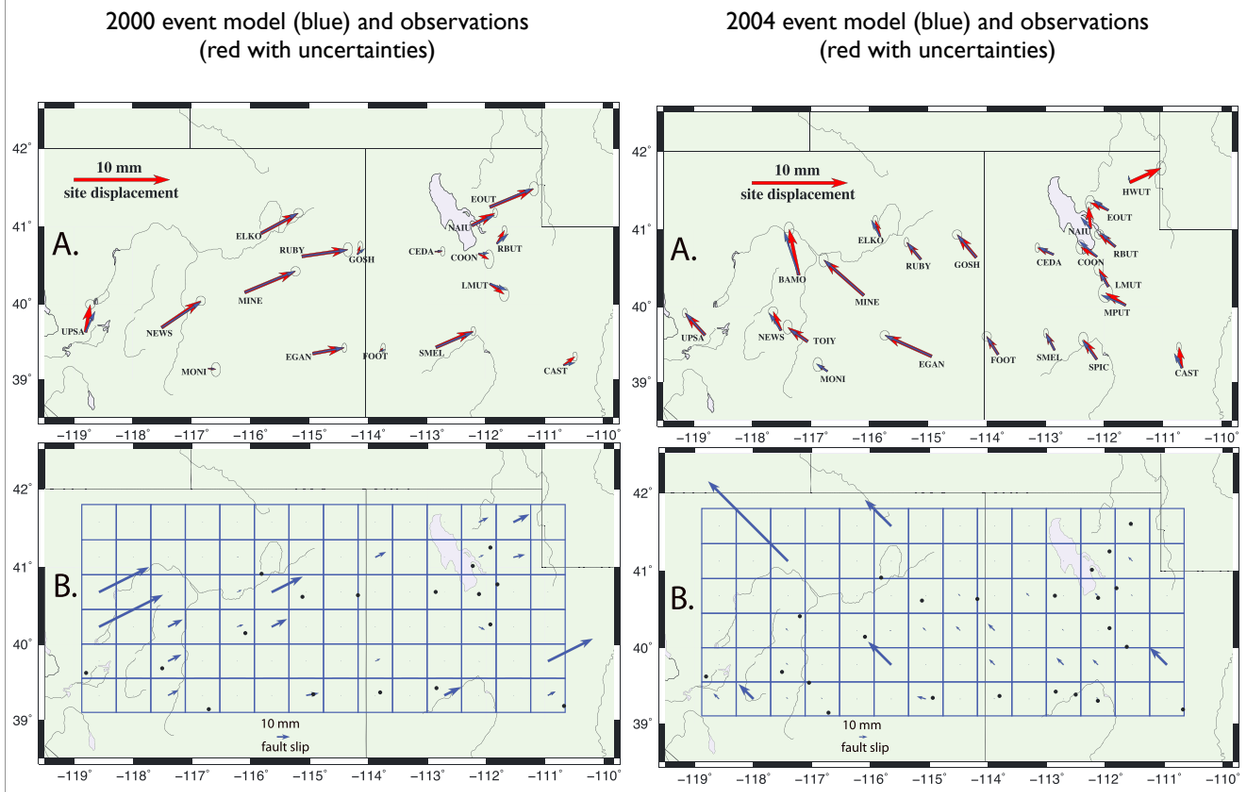

Chamoli et al., JGR, 2014

Modeling this suggests more localized displacement on fairly shallow structures; authors allow that this does still resemble the kind of episodic motions seen in Cascadia but prefer slip on LANFs as doing things here (